ORNL/CON-149

ornl

OAK
RIDGE
NATIONAL
LABORATORY

UNION
CARBIDE

A Theoretical Analysis of a Kinematic Stirling-Cycle Heat Pump for Space Conditioning Applications

N. Domingo W. L. Jackson
F. C. Chen

OPERATED BY
UNION CARBIDE CORPORATION
FOR THE UNITED STATES
DEPARTMENT OF ENERGY

Printed in the United States of America. Available from
National Technical Information Service
U.S. Department of Commerce
5285 Port Royal Road, Springfield, Virginia 22161
NTIS price codes—Printed Copy: A04 Microfiche A01

This report was prepared as an account of work sponsored by an agency of the United States Government. Neither the United States Government nor any agency thereof, nor any of their employees, makes any warranty, express or implied, or assumes any legal liability or responsibility for the accuracy, completeness, or usefulness of any information, apparatus, product, or process disclosed, or represents that its use would not infringe privately owned rights. Reference herein to any specific commercial product, process, or service by trade name, trademark, manufacturer, or otherwise, does not necessarily constitute or imply its endorsement, recommendation, or favoring by the United States Government or any agency thereof. The views and opinions of authors expressed herein do not necessarily state or reflect those of the United States Government or any agency thereof.

ORNL/CON-149
Dist. Category UC-95d

A THEORETICAL ANALYSIS OF A KINEMATIC STIRLING-CYCLE HEAT PUMP FOR SPACE CONDITIONING APPLICATIONS

N. Domingo*
Engineering Technology Division

W. L. Jackson
Computer Sciences Division

F. C. Chen
Energy Division

*On loan to the Energy Division

Date Published - March 1984

Prepared by the
OAK RIDGE NATIONAL LABORATORY
Oak Ridge, Tennessee 37831
operated by
UNION CARBIDE CORPORATION
for the
U.S. DEPARTMENT OF ENERGY
under Contract No. W-7405-eng-26

CONTENTS

Page

LIST OF FIGURES v

LIST OF TABLES vii

ACKNOWLEDGMENTS ix

ABSTRACT 1

1. INTRODUCTION 1

2. SUMMARY 3

3. CONCEPTUAL SYSTEM DESIGN 5

3.1 Selection of Stirling-Cycle Machine for Residential Heat Pump Modeling 5

3.2 Heat Exchangers 5

3.3 Modified Heat Exchangers 12

4. THE COMPUTER MODEL 16

5. RESULTS FROM HEAT PUMP MODELING 19

5.1 Effect of Working Fluid and Source Temperature 19

5.2 Effect of Heat Exchanger Configuration 21

5.3 Parametric Analysis with Modified Heat Exchangers 23

5.3.1 Effects of Source (Outdoor Air) Temperature 27
5.3.2 Effects of Mean Compression-Space Pressure 28
5.3.3 Effects of Crank Speed 28

5.4 Heat Exchanger Sensitivity Analysis 28

5.4.1 Effect of Heat Transfer Fluid Flow Passes 30
5.4.2 Effect of Heat Transfer Fluid Flow Rate 31
5.4.3 Effect of Heat Exchanger Tube Number 33
5.4.4 Effect of Heat Exchanger Tube Length 35
5.4.5 Effect of Heat Rejector-Side Heat Transfer Fluid Inlet Temperature 36
5.4.6 Effect of Temperature Difference Between Outdoor Air and Absorber-Side Heat Transfer Fluid Inlet Temperature 36

REFERENCES 38

Appendix A. INTRODUCTION TO STIRLING-CYCLE HEAT PUMPS 39

Appendix B. SI CONVERSION FACTORS 43

LIST OF FIGURES

Figure		Page
1	Photograph of the GPU-3 engine	6
2	Schematic of the Stirling-cycle heat pump	8
3	Schematic of the working space as built by General Motors	8
4	Cylinder head assembly with gas-to-gas heat absorber	9
5	Heat rejector cartridges	10
6	Stirling-cycle heat pump system integration	12
7	Heat and mass transfer control volumes in NASA computer model	16
8	Outline of computer calculation procedure	18
9	Stirling-cycle heat pump performance for helium and hydrogen: (*a*) COP as function of ambient air temperature and (*b*) heat output as function of ambient air temperature	20
10	Performance for three heat exchanger configurations using hydrogen: (*a*) COP as function of ambient air temperature and (*b*) heat output as function of ambient air temperature	22
11	Performance with modified heat exchangers as function of ambient air temperature and mean compression-space pressure at crank speed of 1800 rpm	24
12	Performance with modified heat exchangers as function of ambient air temperature and mean compression-space pressure at crank speed of 3000 rpm	25
13	Performance with modified heat exchangers as function of crank speed and mean compression-space pressure at crank speed of 3600 rpm	26
14	Performance with modified heat exchangers as function of crank speed and mean compression-space pressure	27
15	Sensitivity of heat exchanger shell-side flow passes	29
16	Sensitivity of heat transfer fluid flow rate	30

Figure		Page
17	Sensitivity of heat exchanger tube number increase	31
18	Sensitivity of heat exchanger tube length increase	32
19	Sensitivity of changes in heat rejector-side heat transfer fluid inlet temperature	33
20	Sensitivity of ambient air temperature to heat absorber-side heat transfer fluid inlet temperature ...	34
A.1	Typical Stirling-cycle heat pump	40
A.2	Stirling-cycle heat pump: (*a*) P-V and T-S diagrams and (*b*) piston positions at state points of the cycle	40

LIST OF TABLES

Table		Page
1	GPU-3 engine dimensions and design parameters	7
2	Dimensions of heat exchangers modeled	14

ACKNOWLEDGMENTS

The work reported here was part of a general program concerning Stirling-Cycle Heat Pump Technology undertaken at Oak Ridge National Laboratory (ORNL) for the Department of Energy (DOE), Energy Conversion Equipment Branch. Ron Fiskum served as Program Manager for DOE and F. A. Creswick (Energy Division) as Technical Manager for ORNL.

The authors appreciate the assistance of many ORNL staff members and are particularly grateful for the contributions of the following people: F. A. Creswick, Technical Manager, Energy Division; V. O. Haynes, Energy Division; J. W. Michel, Section Head, Energy Division; and members of the Engineering Technology Division Publications Office and Word Processing Center for assistance in preparing the manuscript for publication.

The authors are also indebted to R. C. Tew and L. G. Thieme of NASA Lewis Research Center for their guidance in the use of the NASA computer code.

A THEORETICAL ANALYSIS OF A KINEMATIC STIRLING-CYCLE HEAT PUMP FOR SPACE CONDITIONING APPLICATIONS

N. Domingo W. L. Jackson
F. C. Chen

ABSTRACT

A computer simulation was performed for a kinematic Stirling-cycle heat pump (modified from the GPU-3 heat engine mode) using the NASA Lewis Research Center (LERC) third-order code, which employs nodal analysis to solve numerically the governing differential equations. Parametric and sensitivity analyses were carried out to determine the effects of outdoor air (source) temperature, mean compression-space pressure, crank speed, and heat exchanger design parameters on the performance of the Stirling-cycle heat pump. For the modified Stirling-cycle heat pump, the indicated heating coefficient of performance (COP), which excluded mechanical and parasitic losses, ranged from 2.14 to 2.53 for outdoor air temperatures between 255.2 K (0°F) and 281.3 K (47°F), respectively. It was determined from the parametric study that, unlike typical vapor compression cycles, the Stirling-cycle COP and heat capacity were relatively insensitive to outdoor air temperature. These results suggest the possible application of the Stirling-cycle heat pump in colder climates.

1. INTRODUCTION

Stirling-cycle machines in the past were developed mainly as heat engines for power generation[1] and as cryocoolers for ultralow-temperature refrigeration and gas liquefaction. Vapor compression Rankine cycle heat pumps driven by electrical motors, which are by far the most efficient residential space conditioning devices in mild climates, dominate the marketplace.

However, the steady-state performance of a vapor compression heat pump drops rapidly as the ambient (outdoor) air temperature drops.[2] Its seasonal performance is further deteriorated by duty cycling loss at mild ambient temperature, by losses of frosting of the outdoor coil, and by cycle reversal to defrost at freezing ambient temperature. Supplemental

heating from such sources as electric resistance elements is needed to meet the heating load at low outdoor temperatures.

An alternative heat pump cycle study[3] has been done to evaluate various heat pump cycles for space conditioning applications that might offer improved performance over the basic vapor compression cycle concept. The Stirling-cycle heat pump (see Appendix A), which offers a number of potential advantages including high efficiency, low sensitivity to heat source temperature, ease of defrosting, and capacity modulation by pressure control, was identified as a promising alternative heat pump concept.

The Stirling-cycle machine has long been proven to be cost-effective for cryogenic applications. Its potential applicability in the residential space conditioning field has only recently been explored. To substantiate the potential advantages, a computer simulation of a kinematic Stirling-cycle heat pump for residential space conditioning is reported in this paper. Results of the parametric and sensitivity analyses are reported to further delineate the effects of various design parameters on the performance of a kinematic Stirling-cycle heat pump.

2. SUMMARY

The main results of this analysis on a Stirling-cycle heat pump may be summarized as follows:

1. The General Motors Stirling-cycle GPU-3 heat engine was modeled to operate as a heat pump (heating mode) by converting the heat absorber to a shell-and-tube design for better transfer of heat from outdoor air to the working gas.

2. For the modified Stirling-cycle heat pump, the indicated coefficient of performance (COP) ranged from 2.14 to 2.53 for outdoor air temperatures between 255.2 K (0°F) and 281.3 K (47°F) respectively. For this temperature range, heat capacity ranged from 5.1 kW (17,400 Btu/h) to 4.9 kW (16,724 Btu/h). The above performance was obtained with adiabatic expansion and compression spaces, using hydrogen at a mean gas pressure of 2.76 MPa (400 psi) and a crank speed of 1800 rpm for an assumed temperature difference of 8.3 K (15°F) between outdoor air and heat absorber-side fluid inlet temperature.

3. From the parametric studies it was found that, unlike the vapor compression cycles, both the COP and heating capacity were relatively insensitive to outdoor air temperature. For a fixed mean gas pressure and crank speed, the indicated COP increased up to 10%, while heat capacity decreased by ~3% for outdoor air temperatures between 264.7 K (17°F) and 281.3 K (47°F).

4. From the same parametric studies, it was found that COP decreased while heat capacity increased with increasing mean gas pressure and/or crank speed. For a fixed outdoor air temperature and crank speed, indicated COP decreased to ~10%, and heat capacity increased by a factor of 2 when mean gas pressure was increased from 2.76 to 5.52 MPa (400 to 800 psi). Similarly, for a fixed outdoor air temperature and mean gas pressure, indicated COP decreased by ~28%, and heat capacity increased by a factor of 2.2 when crank speed was increased from 1800 to 3600 rpm.

5. For the same operating conditions, the COP predicted with the hydrogen working fluid was 25% greater than with helium, yet the heat capacity decreased by 24%.

6. Results from sensitivity analyses performed on the heat absorber and heat rejector heat exchangers showed that changes in tube number and tube length had a significant effect on COP and heat capacity for a given set of operating conditions. This may have been attributed to changes in heat exchanger dead volume, which affects gas compression ratio and flow friction.

7. Increasing the number of tubes in the heat rejector by 50% increased COP by 5.5% and decreased heat capacity by 5.4%.

3. CONCEPTUAL SYSTEM DESIGN

3.1 Selection of Stirling-Cycle Machine for Residential Heat Pump Modeling

The General Motors Ground Power Unit 3 (GPU-3) Stirling-cycle engine[4] was chosen for investigating the potential of Stirling-cycle heat pumps for residential heating in this study. Selection of the GPU-3 engine for heat pump modeling was based on the following factors:

1. It incorporates a simple engine design.
2. Dimensional and performance data[5,6] as a heat engine are nonproprietary.
3. The computer code used for simulation is tailored specifically for the GPU-3 engine and validated by NASA against GPU-3 performance test data.

Figure 1 shows a photograph of the GPU-3 unit, as originally built for the U.S. Army in 1965 as an engine generator. Table 1 gives dimensions and design performance characteristics of the GPU-3 engine.

Figure 2 shows a schematic of the Stirling-cycle heat pump. Movement of the displacer piston does not change the total volume of the working fluid; its purpose is to move the gas through heat exchangers and regenerators in a periodic fashion. However, movement of the power piston will cause a change in gas volume. The rhombic drive motion may be seen in Fig. 2 from the views of the drive given in two positions.

A schematic of the working space as built by General Motors is illustrated in Fig. 3. A photograph of the cylinder head assembly with the heat absorber is shown in Fig. 4. Figure 5 shows a heat rejector cartridge (a total of eight cartridges are used in the GPU-3).

3.2 Heat Exchangers

Martini[7] has stated that the technology of how to add and remove heat from the working fluid in a Stirling-cycle engine is the most crucial of the entire engine designs. Serious though the heat transfer problems may be for heat engine development, they are even more important for heat pump

ORNL–PHOTO 2597–83

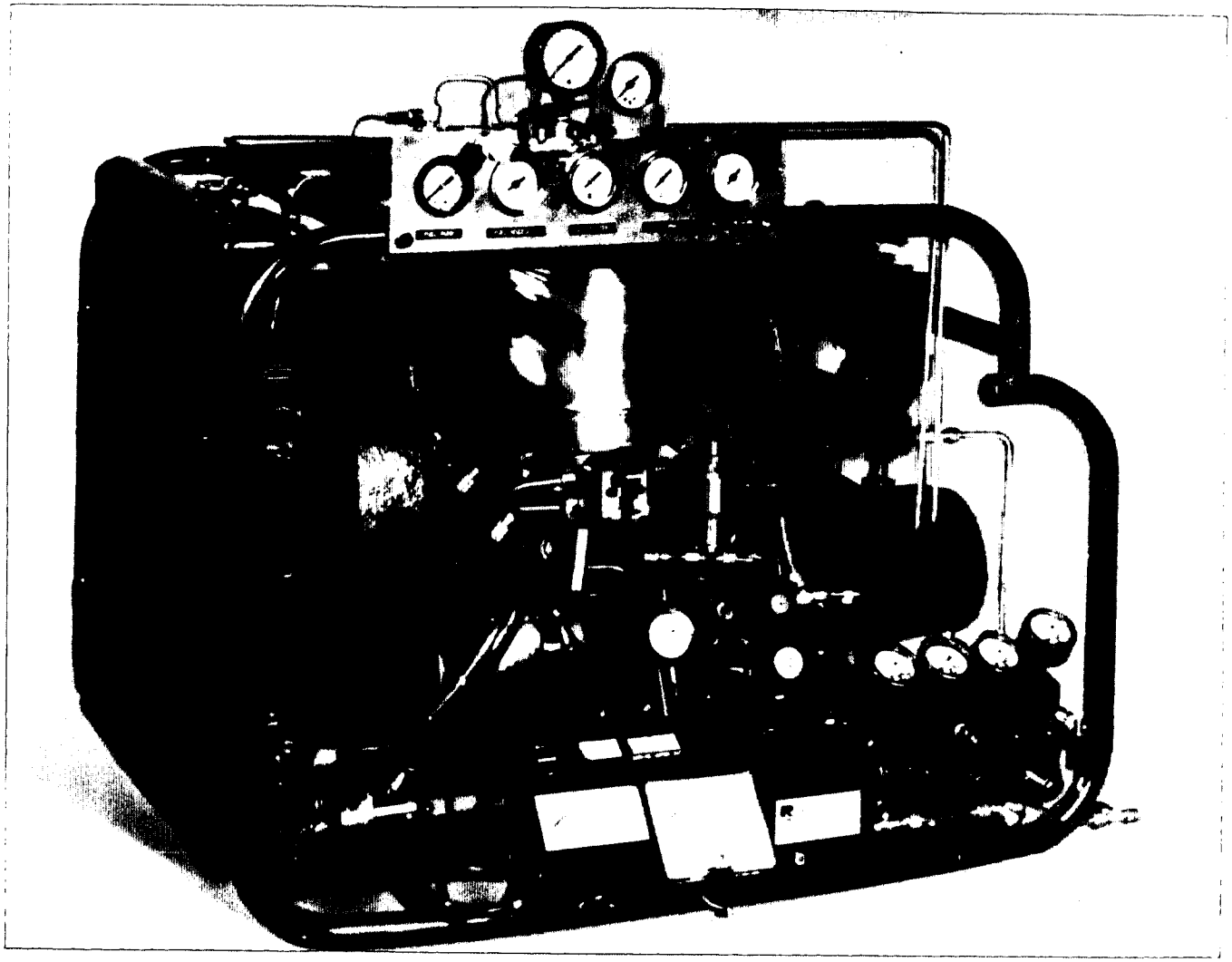

Fig. 1. Photograph of the GPU-3 engine. *Source*: NASA Lewis Research Center.

Table 1. GPU-3 engine dimensions and design parameters

Number of cylinders	1
Type of engine	Displacer
Type of drive	Rhombic
Type of shaft seals	Sliding
Miscellaneous:	
Cylinder bore with liner, cm (in.)	6.99 (2.75)
Cylinder bore above liner (top of displacer seal at top of liner at displacer top-dead-center), cm (in.)	7.01 (2.76)
Stroke, cm (in.)	3.15 (1.24)
Displacement (maximum change in total working-space volume), cm^3 ($in.^3$)	119.6 (7.30)
Piston-rod diam, cm (in.)	2.22 (0.875)
Displacer-rod diam, cm (in.)	0.953 (0.375)
Displacer diam, cm (in.)	6.96 (2.74)
Displacer wall thickness, cm (in.)	0.159 (0.0625)
Expansion-space clearance, cm (in.)	0.163 (0.064)
Compression-space clearance, cm (in.)	0.030 (0.012)
Drive:	
Connecting-rod length, cm (in.)	4.60 (1.81)
Crank radius, cm (in.)	1.38 (0.543)
Eccentricity, cm (in.)	2.08 (0.82)
Working fluid	Hydrogen (H_2)
Design speed (heat engine)	3000 rpm
Design pressure (heat engine)	6895 kPa (1000 psi)
Design output (heat engine)	8.0 net brake hp
Design efficiency (heat engine)	26.5%

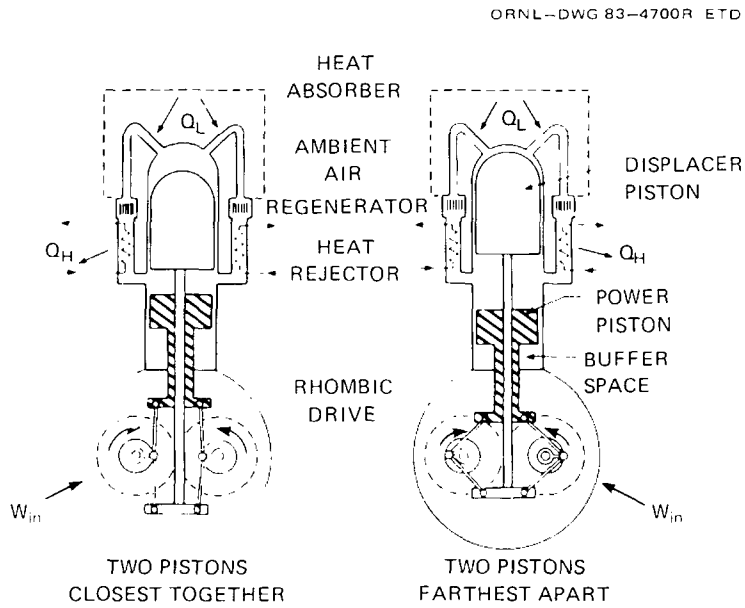

Fig. 2. Schematic of the Stirling-cycle heat pump.

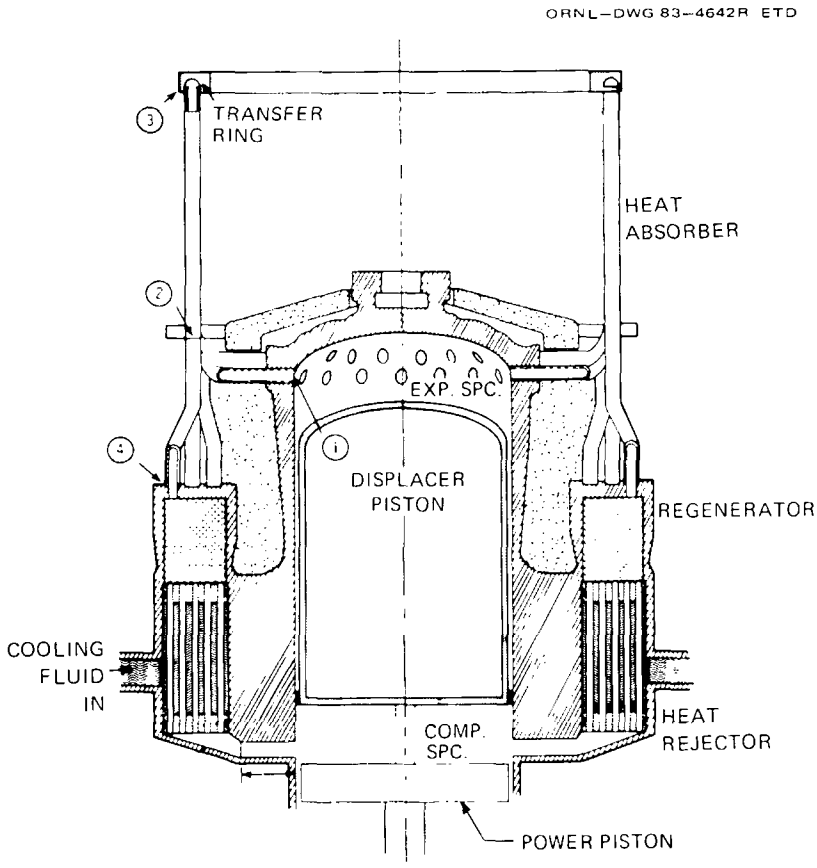

Fig. 3. Schematic of the working space as built by General Motors. *Source*: W. R. Martini, *Stirling Engine Design Manual*, NASA CR-135382, April 1978.

ORNL–PHOTO 1920–83

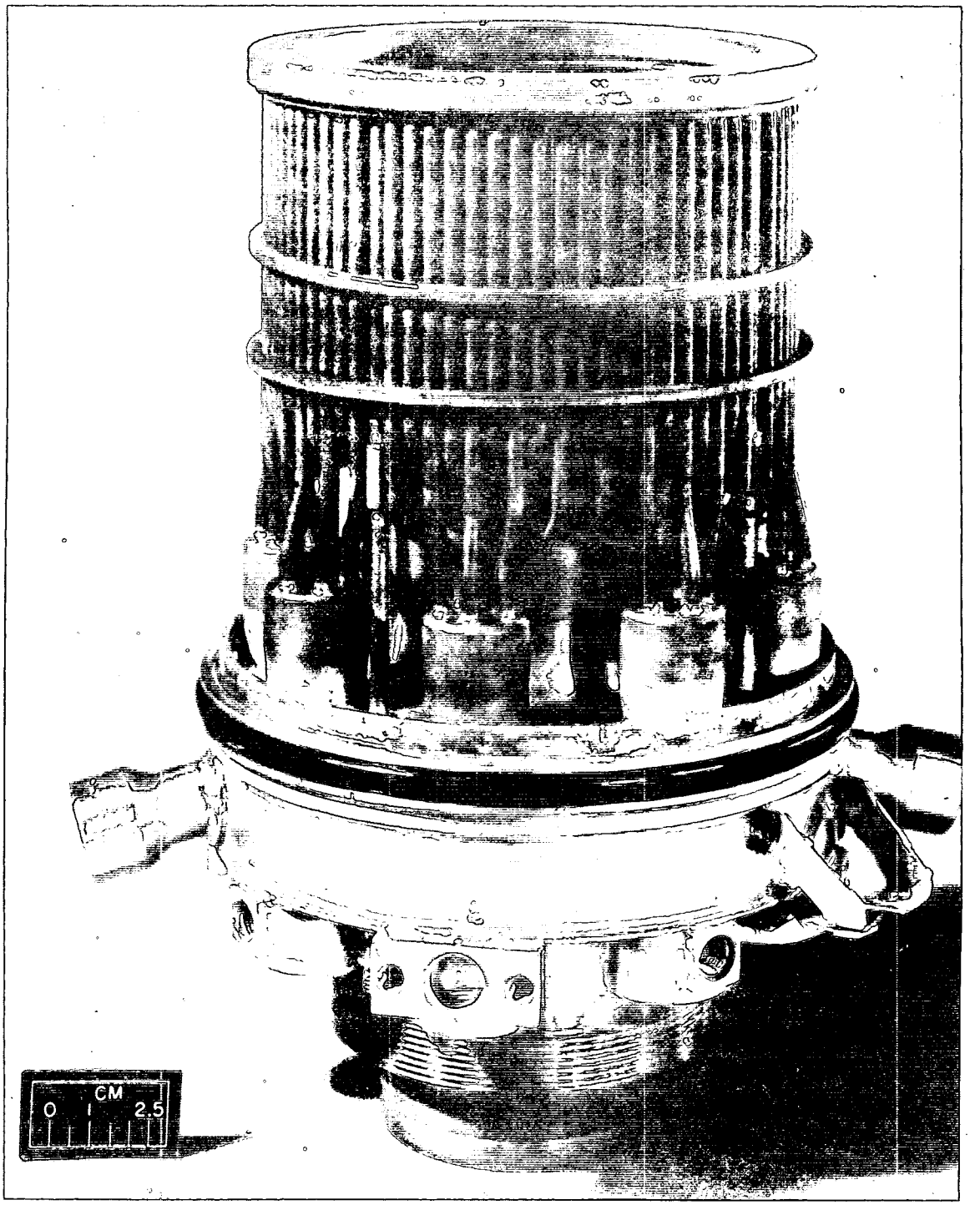

Fig. 4. Cylinder head assembly with gas-to-gas heat absorber.
Source: NASA Lewis Research Center.

ORNL-PHOTO 1919-83

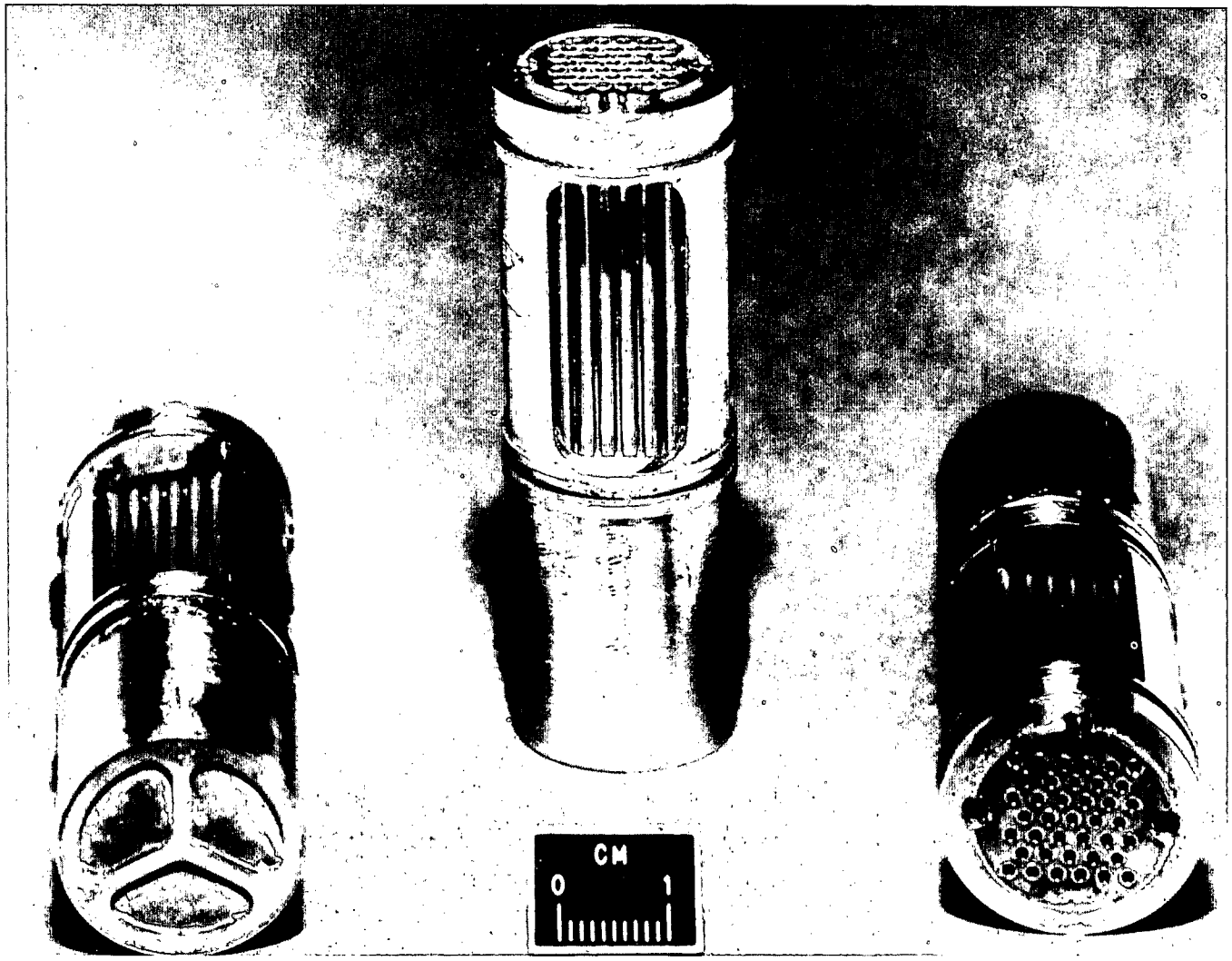

Fig. 5. Heat rejector cartridges. *Source*: NASA Lewis Research Center.

development because of the smaller temperature difference between the heat absorber and heat rejector portions of the heat pump. In typical Stirling-cycle engines, the hot and cold spaces in which isothermal expansion and compression processes are to occur do not remain isothermal. In reality, these spaces are more nearly adiabatic than isothermal. This adiabatic effect is most serious when a Stirling-cycle engine operates over a small temperature difference.[8] In other words, for the case of a heat pump, more power will be required than if the spaces were isothermal. Thus, emphasis is required to make the compression and expansion processes isothermal, as the ideal cycle calls for. This can be achieved by the design and development of high-performance heat exchangers and regenerators.[9,10] These components must be designed not only for enhanced heat transfer, but for low pressure losses and dead volumes,* which tend to increase the power input required per cycle. On the basis of the above remarks and the fact that the GPU-3 heat exchangers were designed for heat engine operation, it was decided to investigate only heat exchangers in this study. Because of time constraints, the GPU-3 regenerator was not investigated.

As a residential heat pump, the original GPU-3 heat absorber does not have a suitable design for absorbing heat from ambient outdoor air to the working gas because of the poor heat transfer mechanism existing between the outdoor air, heater wall, and working gas. Unlike the heat absorber, the heat rejector (Fig. 5) configuration is of the shell-and-tube design, which allows for the flow of a heat transfer fluid to transfer the heat from the working gas to ambient. In the case of a heat pump, heat transfer fluid from the heat rejector may be circulated through an indoor coil to provide heat to a conditioned space. It becomes clear, then, that conversion of the GPU-3 to a heat pump requires the modification of the existing heat absorber to a configuration more suitable for transferring heat from the surroundings. As for the heat rejector, a shell-and-tube configuration for the heat absorber will allow for the flow of a heat

*Dead volume refers to the total internal volume of the heat exchangers, regenerators, and associated ducts and ports.

transfer fluid to provide a temperature source to the working gas. The fluid may be circulated through an appropriate outdoor coil and heated by outdoor air. Figure 6 shows a schematic of a possible Stirling-cycle heat pump system.

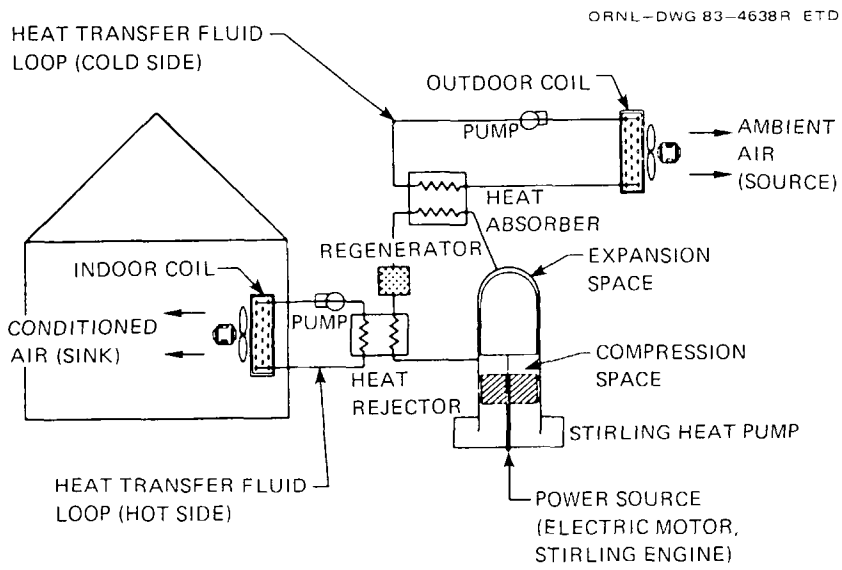

Fig. 6. Stirling-cycle heat pump system integration.

3.3 Modified Heat Exchangers

An improved heat absorber design was analytically modeled into the NASA computer program to replace the original heat absorber configuration. As noted earlier, this was necessary because the original heat absorber was designed as a gas-to-gas type heat exchanger. In order to keep a similar cylinder head configuration, the heat exchanger chosen was similar to the existing heat rejector design (Fig. 5) which consisted of 8 cartridges of 39 small-diameter round tubes in a shell-and-tube configuration. Like the heat rejector, the new heat absorber used 8 cartridges of 39 round tubes with identical flow conditions existing in each of the 8 parallel flow paths. For the shell-side heat transfer fluid, a circulating mixture of water and 50% ethylene glycol was assumed for both heat absorber and heat rejector because the circulating fluid would be exposed to

air temperatures below the freezing point of water during heat pump operation. In addition, the mixture of water and ethylene glycol is cheap and safe, with good heat transfer properties.

The heat exchangers were categorized as follows: (1) Base Case I would be the original heat absorber—regenerator—heat rejector configuration, (2) Base Case II would utilize the modified heat absorber design with the existing regenerator and heat rejector of Base Case I, and (3) Base Case III would be upgraded versions of the heat absorber and heat rejector used in Base Case II as prescribed by results obtained from sensitivity studies presented in Sect. 5.4.

For the heat exchanger sensitivity study, several heat exchanger design parameters were investigated. These included (1) shell-side flow passes for the heat transfer fluid, (2) heat transfer fluid flow rates, (3) tube number, and (4) tube length. These parameters were chosen because they improve heat transfer by increasing shell-side and tube-side heat transfer coefficients and effective heat transfer area.

Table 2 gives the dimensions of Base Case I, II, and III heat exchangers which were used for computer simulation of the Stirling-cycle heat pump. For the heat absorber an 18% increase in gas-side heat transfer area and a 73% decrease in dead volume is noted between Base Cases I and II in Table 2. For the heat rejector, dimensions are the same for Base Cases I and II. In Base Case III, shell-side flow passes for both the heat absorber and heat rejector are doubled. Except for an increase in shell-side flow passes, the heat absorber dimensions for Base Case III are identical to those for Base Case II. However, in Base Case III, the heat rejector heat transfer area and dead volume are increased 50 and 39%, respectively.

Table 2. Dimensions of heat exchangers modeled

	Base Case		
	I	II	III
Heat absorber			
Tube length, cm (in.)	24.23 (9.54)[a]	6.51 (2.564)	6.51 (2.564)
Heat transfer length, cm (in.)	15.54 (6.12)[a]	5.46 (2.15)	5.46 (2.15)
Tube inside diam, cm (in.)	0.302 (0.119)	0.108 (0.0425)	0.108 (0.0425)
Tube outside diam, cm (in.)	0.483 (0.190)	0.159 (0.0625)	0.159 (0.0625)
Total surface area (gas-side), cm^2 ($in.^2$)	490.58 (76.035)	577.83 (89.564)	577.83 (89.564)
Total dead volume, cm^3 ($in.^3$)	68.42 (4.175)	18.60 (1.135)	18.60 (1.135)
Number of cartridges in cylinder head	8	8	8
Number of tubes per cartridge	5	39	39
Total number of tubes	40[b]	312	312
Shell-side flow passes	c	1	2
Heat transfer fluid flow rate, m^3/s (gpm)	c	6.31×10^{-4} (10)	6.31×10^{-4} (10)
Heat rejector			
Tube length, cm (in.)	4.60 (1.81)	4.60 (1.81)	6.38 (2.512)
Heat transfer length, cm (in.)	3.56 (1.40)	3.56 (1.40)	5.33 (2.10)
Tube inside diam, cm (in.)	0.108 (0.0425)	0.108 (0.0425)	0.108 (0.0425)
Tube outside diam, cm (in.)	0.159 (0.0625)	0.159 (0.0625)	0.159 (0.0625)
Total surface area (gas-side), cm^2 ($in.^2$)	375.95 (58.27)	375.95 (58.27)	563.92 (87.41)
Total dead volume, cm^3 ($in.^3$)	13.13 (0.801)	13.13 (0.801)	18.21 (1.111)
Number of cartridges in cylinder head	8	8	8
Number of tubes per cartridge	39	39	39
Total number of tubes	312	312	312
Shell-side flow passes	1	1	2
Heat transfer fluid flow rate, m^3/s (gpm)	6.31×10^{-4} (10)	6.31×10^{-4} (10)	6.31×10^{-4} (10)

Table 2 (continued)

	Base Case		
	I	II	III
Regenerator (same dimensions for Base Cases I, II, and III)			
Length (inside), cm (in.)	2.26 (0.89)		
Diam (inside), cm (in.)	2.26 (0.89)		
Number of cartridges in cylinder head	8		
Total surface area, m^2 ($in.^2$)	2.16 (3355.20)		
Total dead volume, cm^3 ($in.^3$)	65.51 (3.998)		
Matrix:			
Wire-cloth material	304 stainless steel		
Cloth mesh per 2.54 cm (1 in.)	200 x 200		
Wire diam, cm (in.)	0.00406 (0.0016)		
Number of layers	308		
Filler factor, %	30.3		

[a]3.33 cm (1.31 in.) completely insulated between 1 and 2; 7.77 cm (3.06 in.) from 2 up to 3; 7.77 cm (3.06 in.) from 3 down to 2; 5.33 cm (2.098 in.) completely insulated from 2 down to 4 (See heat absorber tube schematic in Fig. 3 for definition of locations 1 through 4.)

[b]Five heat absorber tubes per heat rejector—regenerator cartridge (a total of eight).

[c]Since original design heat absorber was a gas-to-gas heat exchanger, no shell-side flow passes existed.

4. THE COMPUTER MODEL

The third-order computer model used to calculate the performance of a Stirling-cycle heat pump is a modified version of a Stirling-cycle engine computer model written by NASA.[11] The model, tailored specifically to the GPU-3 engine, is based on the assumption that identical flow conditions exist in each of the eight parallel flow paths through the heat rejector units. The model represents the working space and metal walls by a series of control volumes.

The model divides the heat pump into 13 subdivisions, called control volumes, representing the working space: 1 for the expansion space, 3 for the heat absorber, 5 for the regenerator, 3 for the heat rejector, and 1 for the compression space, as shown in Fig. 7. The adjacent metal walls are represented by 13 corresponding control volumes. All metal temperatures, except for the regenerator, are assumed to remain constant for a given run since the heat absorber and heat rejector metal temperatures are essentially boundary temperatures controlled by the heating and cooling heat transfer fluid temperatures and flow rates.

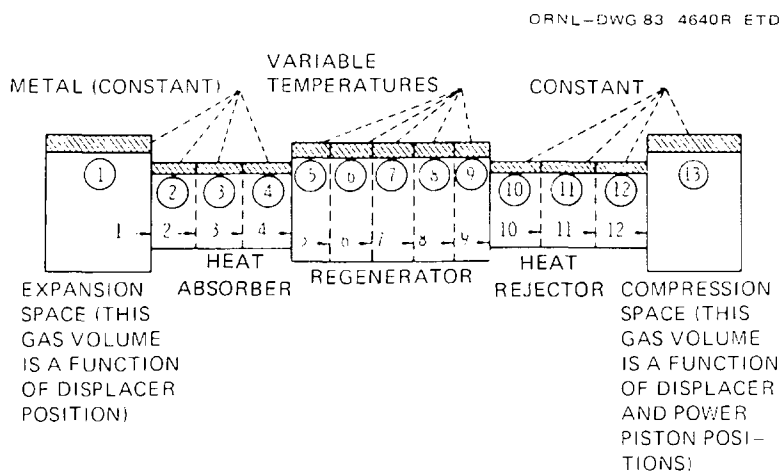

Fig. 7. Heat and mass transfer control volumes in NASA computer model. *Source*: R. Tew, K. Jeffries, and D. Miao, *A Stirling Engine Computer Model for Performance Calculations*, DOE/NASA TM-78884, U.S. DOE, July 1978.

The combustion heat absorber design was replaced by a heat exchanger design in the model with a similar configuration to the heat rejector design, with eight cartridges of tubes placed on top of the regenerator in place of the heat absorber head. The fixed metal temperatures for the heat absorber and heat rejector are determined in an iterative process since they depend on heat transfer fluid flow rates, inlet temperatures, and heat absorption/rejection rates, which, in turn, depend on the metal temperatures. The built-in design parameters describing heat exchanger geometry were changed to input parameters to facilitate optimization of design for a heat pump.

Output from the model includes

1. basic heat output delivered to the space heating water—ethylene glycol loop, including heat transfer in the heat rejector and compression space;
2. basic indicated power input and COP, which exclude losses;
3. indicated power input and COP, which include working fluid flow friction losses; and
4. total indicated power input and net COP, which include working fluid flow friction losses, mechanical friction losses, and water—ethylene glycol pumping power losses through the heat absorber and heat rejector.

The model also simulates temperature, pressure, and flow variations over the cycle at various places in the working space.

The thermodynamic equations and assumptions used in the model were reported by NASA.[11] The overall computational scheme is shown in Fig. 8. Each set of calculations indicated in Fig. 8 within the inner loop (except for pressure-drop, conduction, and shuttle losses) is made at each integration time step during each cycle. It is necessary to make the pressure drop calculations only over the last cycles where they are needed for the output results since, as explained by NASA,[11,12] the pressure drop calculations are decoupled from the heat and mass transfer calculations. Conduction and shuttle losses are calculated only during the last cycles. Revision of regenerator, heat absorber tube, and heat rejector tube metal temperatures is done once per cycle up to a specified number of cycles.

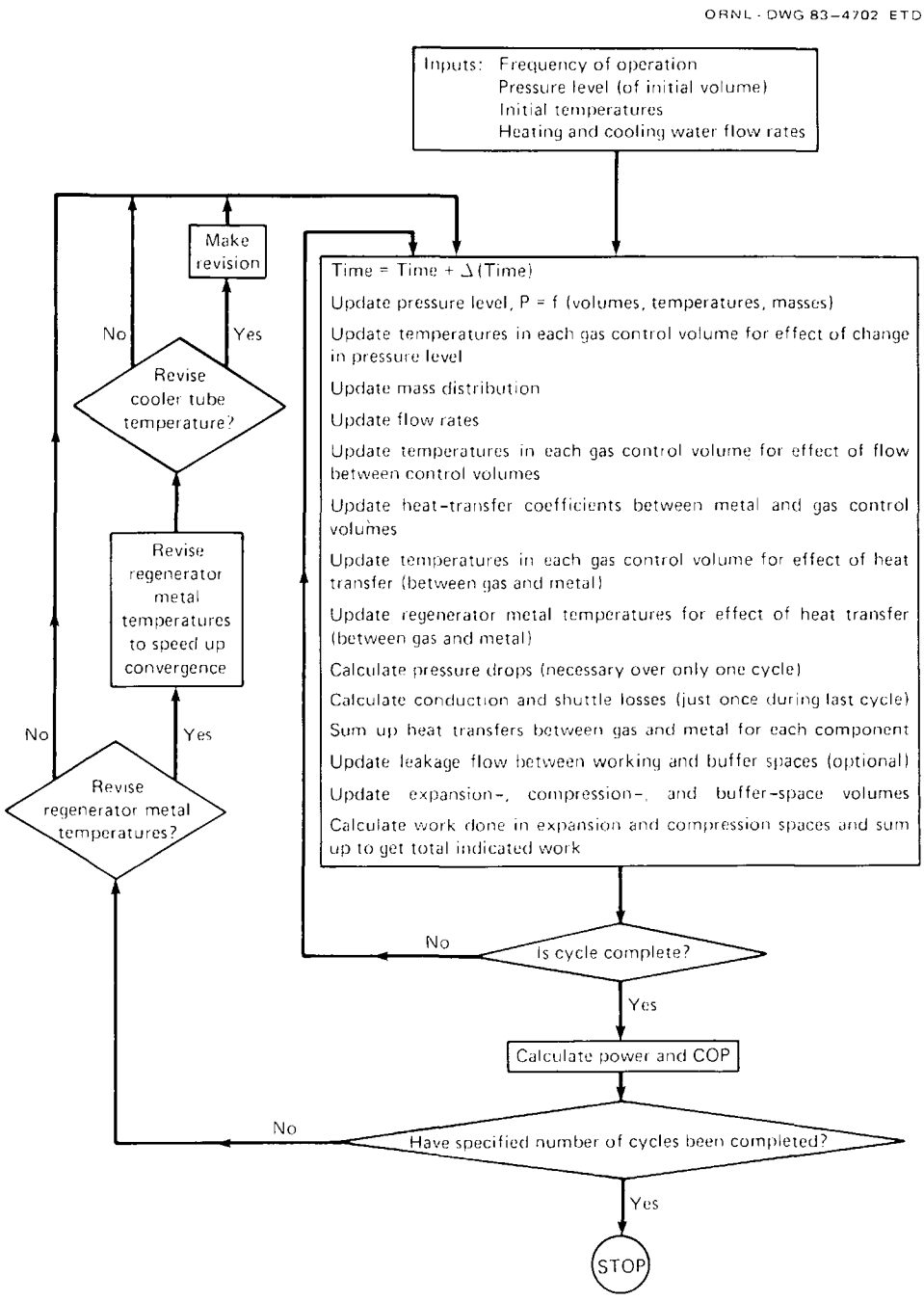

Fig. 8. Outline of computer calculation procedure. *Source*: R. Tew, K. Jeffries, and D. Miao, *A Stirling Engine Computer Model for Performance Calculations*, DOE/NASA TM-78884, U.S. DOE, July 1978.

With these temperatures converged, the calculations proceed another five cycles to allow the further stabilization from one cycle to the next. The run is then complete.

5. RESULTS FROM HEAT PUMP MODELING

The following sections present the most important results from the computer simulations. A comparison of Stirling-cycle heat pump performance is made with hydrogen and helium as the working fluid. The effect of modified heat exchanger configurations on heat pump performance is investigated. Individual discussions are arranged for the parametric and sensitivity studies carried out with the Stirling-cycle heat pump.

The parametric study served to determine the effect of Stirling-cycle heat pump performance with changes in mean compression-space pressure (mean gas pressure), crank speed, ambient air (outdoor) temperature, and rejector-side heat transfer fluid inlet temperature. Modifications to the heat exchangers (excluding the regenerator) were made by carrying out a sensitivity study. The sensitivities of changes in (1) heat exchanger tube length, (2) heat exchanger tube number, (3) heat transfer fluid flow passes, (4) heat transfer fluid flow rates, (5) ambient air to absorber-side heat transfer fluid inlet temperature differences, and (6) rejector-side heat transfer fluid inlet temperature to the performance of the Stirling-cycle heat pump were investigated.

5.1 Effect of Working Fluid and Source Temperature

Indicated COP and heat output at a constant crank speed and mean compression-space pressure are shown in Fig. 9 for hydrogen and helium as the working fluid. Indicated COP calculations do not include mechanical friction losses and parasitic losses, such as fans and accessories. The Base Case II heat exchangers (Table 2) were used for the data presented in Fig. 9. Computer runs were made at ambient air (source) temperatures of 264.7, 273, and 281.3 K (17, 32, and 47°F). A temperature difference* of 16.7 K (30°F) between ambient air and absorber-side fluid inlet

*In an outdoor coil of a typical vapor compression heat pump, the temperature difference between the entering air and refrigerant can range from 3.3 K (6°F) to 16.7 K (30°F) (ref. 2). For the Stirling-cycle heat pump, the 16.7 K (30°F) assumption was made in order to initiate the most conservative case for an outdoor coil.

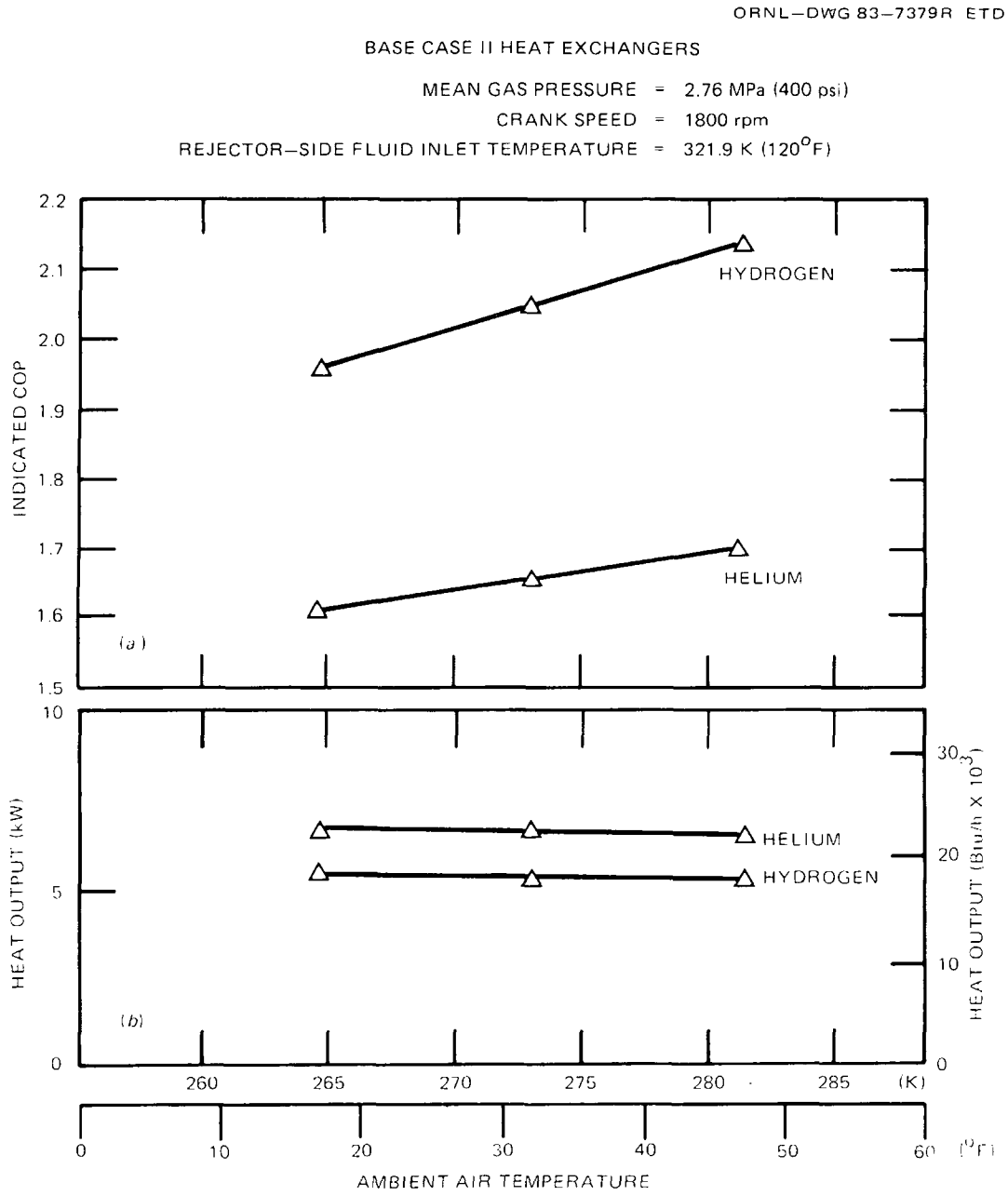

Fig. 9. Stirling-cycle heat pump performance for helium and hydrogen: (*a*) COP as function of ambient air temperature and (*b*) heat output as function of ambient air temperature.

temperature was chosen. The rejector-side fluid inlet temperature was set at 321.9 K (120°F), and the heat transfer fluid flow rate through the heat absorber and heat rejector was fixed at 6.31×10^{-4} m^3/s (10 gpm).

As shown in Fig. 9, COP values increased with increasing ambient temperatures, but heat output values remained fairly constant for the range of temperatures covered. Figure 9 shows that COP is greatly increased by using hydrogen as the working gas; however, a decrease in heat output is noted. At a mean compression-space pressure of 2.76 MPa (400 psi) and speed of 1800 rpm, COP values increased as much as 25% while heat output decreased by about 24% for hydrogen. The increase in COP with hydrogen is mainly attributed to the lower flow losses (low density) through the heat exchangers. The decrease in heat output with hydrogen is due to lower values for heat transfer coefficients between the heat exchanger wall and gas. Hydrogen has the highest thermal conductivity, lowest density, and a low specific heat on a volume basis. Helium has a lower volumetric specific heat than hydrogen and a comparable thermal conductivity, but a density almost twice that of hydrogen.

For ratios of specific heats (k) close to 1, the heat addition and heat rejection processes with variable volumes become nearly isothermal ($PV^k = C$, a constant, defines an isothermal process when $k = 1$). The factor, k, is also an indication why hydrogen ($k = 1.40$) achieved higher COP values than helium ($k = 1.66$) with adiabatic variable volumes.

5.2 Effect of Heat Exchanger Configuration

Simulated Stirling-cycle heat pump data are presented in Fig. 10 for three categories of heat exchanger design (Base Cases I, II, and III, as given in Table 2) investigated. As stated earlier, Base Case I was the original General Motors heat exchanger design (Fig. 4). In Base Case II, the original heat absorber was replaced by a configuration similar to the existing heat rejector (Fig. 5). For Base Case III, the heat absorber and heat rejector were modified to include changes in heat transfer fluid flow passes, tube length, and heat transfer fluid flow rates as directed by results from heat exchanger sensitivity analyses.

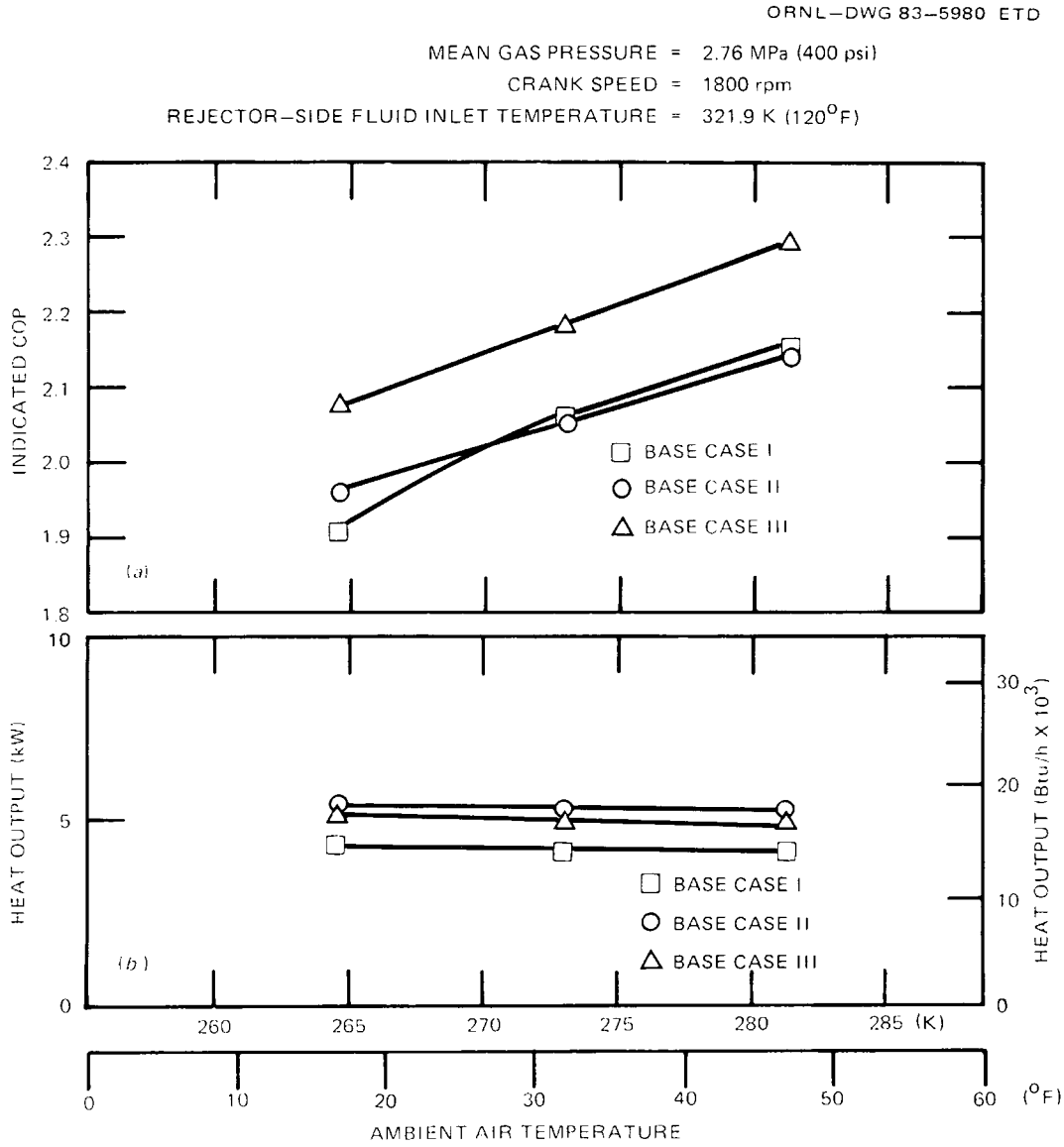

Fig. 10. Performance for three heat exchanger configurations using hydrogen: (*a*) COP as function of ambient air temperature and (*b*) heat output as function of ambient air temperature.

Figure 10 shows COP values for Base Cases I and II to be similar except when ambient air temperatures fall below 269.7 K (26°F). For air temperatures greater than 269.7 K (26°F), the Base Case II configuration yields a slightly higher performance. At the Air Conditioning and Refrigeration Institute (ARI) low rating point of 264.7 K (17°F), the COP is about 3% higher using a Base Case II configuration. The heat output for

Base Case II averages about 25% higher than Base Case I regardless of ambient air temperature. Although the Base Case I and II heat rejector geometries are identical, the new Base Case II heat absorber has an 18% increase in gas-side heat transfer area and a 73% decrease in dead volume when compared with the original Base Case I configuration (see Table 2).

It is clear from Fig. 10 that the Base Case III heat exchanger configuration yielded the best heat pump performance (assuming adiabatic cylinders) for a fixed mean compression-space pressure and crank speed. Values of COP were up to 9% higher than those obtained with the original configuration. The heat output was slightly below that for Base Case I. At the ARI ratings points of 264.7 and 281.3 K (17 and 47°F), the COP ranged from 2.08 to 2.3, respectively, while heat output remained fairly constant at about 5 kW (17,064 Btu/h). For Base Case III, the heat transfer area and dead volume of the heat absorber remained equal to Base Case II values. However, the heat transfer area and dead volume of the heat rejector were increased 50 and 39%, respectively, from Base Case II values. Unlike Base Cases I and II, a two-pass flow arrangement was modeled for the heat transfer fluid circulating through the heat absorber and heat rejector in Base Case III.

As was noted earlier, a temperature difference of 16.7 K (30°F) was chosen between ambient outdoor air temperature and the heat absorber-side fluid inlet temperature. From results obtained in this study it appears that the above assumption was a conservative one, because a higher temperature difference between the hot (compression) space and the cold (expansion) space will exist in the Stirling-cycle heat pump. Consequently, more input work would be required to drive the Stirling-cycle heat pump, thus lowering COP. Figure 20 in Sect. 5.4.6 illustrates this point when the assumed temperature difference between the ambient outdoor air and the heat absorber-side fluid inlet is reduced by half.

5.3 Parametric Analysis with Modified Heat Exchangers

Computer simulation results from a parametric analysis are presented in Figs. 11 through 14. The Base Case III configuration for the heat

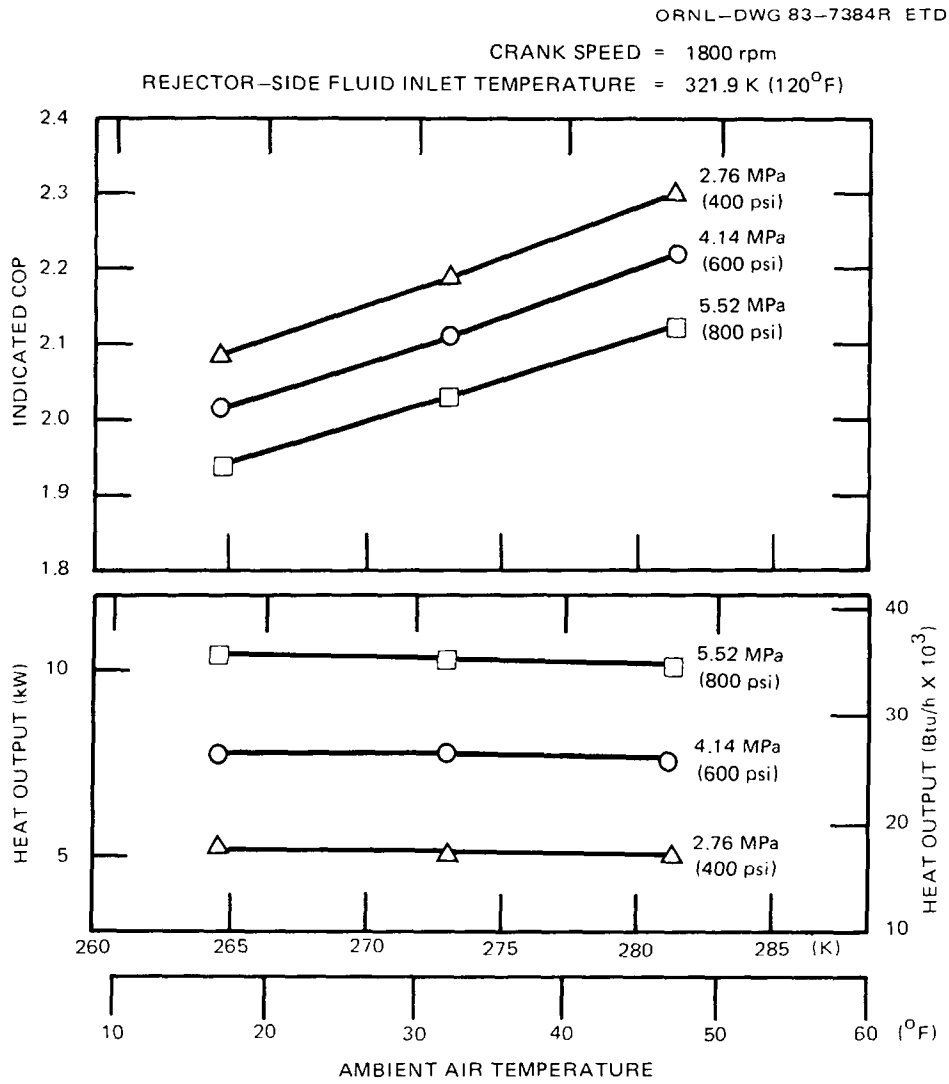

Fig. 11. Performance with modified heat exchangers as function of ambient air temperature and mean compression-space pressure at crank speed of 1800 rpm.

exchangers was employed based on the encouraging results obtained from sensitivity analyses discussed in Sect. 5.4.

Computer runs were performed to map the Stirling-cycle heat pump COP (no mechanical friction losses and parasitic losses included) and heat output over a range of ambient air temperatures, mean compression-space pressures, and crank speeds with hydrogen as the working gas.

Ambient air temperatures of 264.7, 273, and 281.3 K (17, 32, and 47°F) were chosen along with mean compression-space pressures of 2.76,

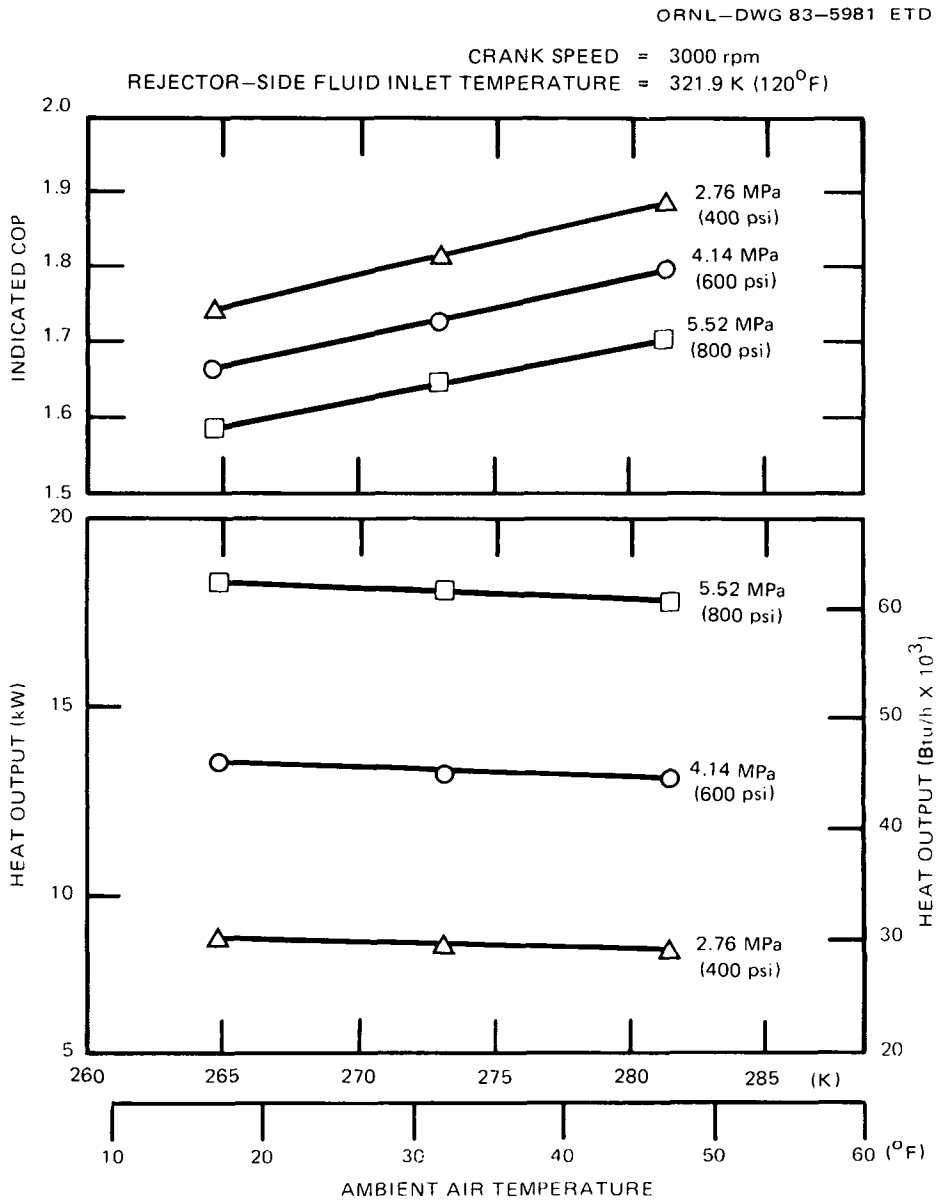

Fig. 12. Performance with modified heat exchangers as function of ambient air temperature and mean compression-space pressure at crank speed of 3000 rpm.

4.14, and 5.52 MPa (400, 600, and 800 psi) and crank speeds of 1800, 3000, and 3600 rpm.

The heat transfer fluid flow rate through the heat absorber and heat rejector was set at 6.31×10^{-4} m^3/s (10 gpm) and the inlet fluid temperature at the heat rejector was 321.9 K (120°F). Again, a 16.7 K (30°F)

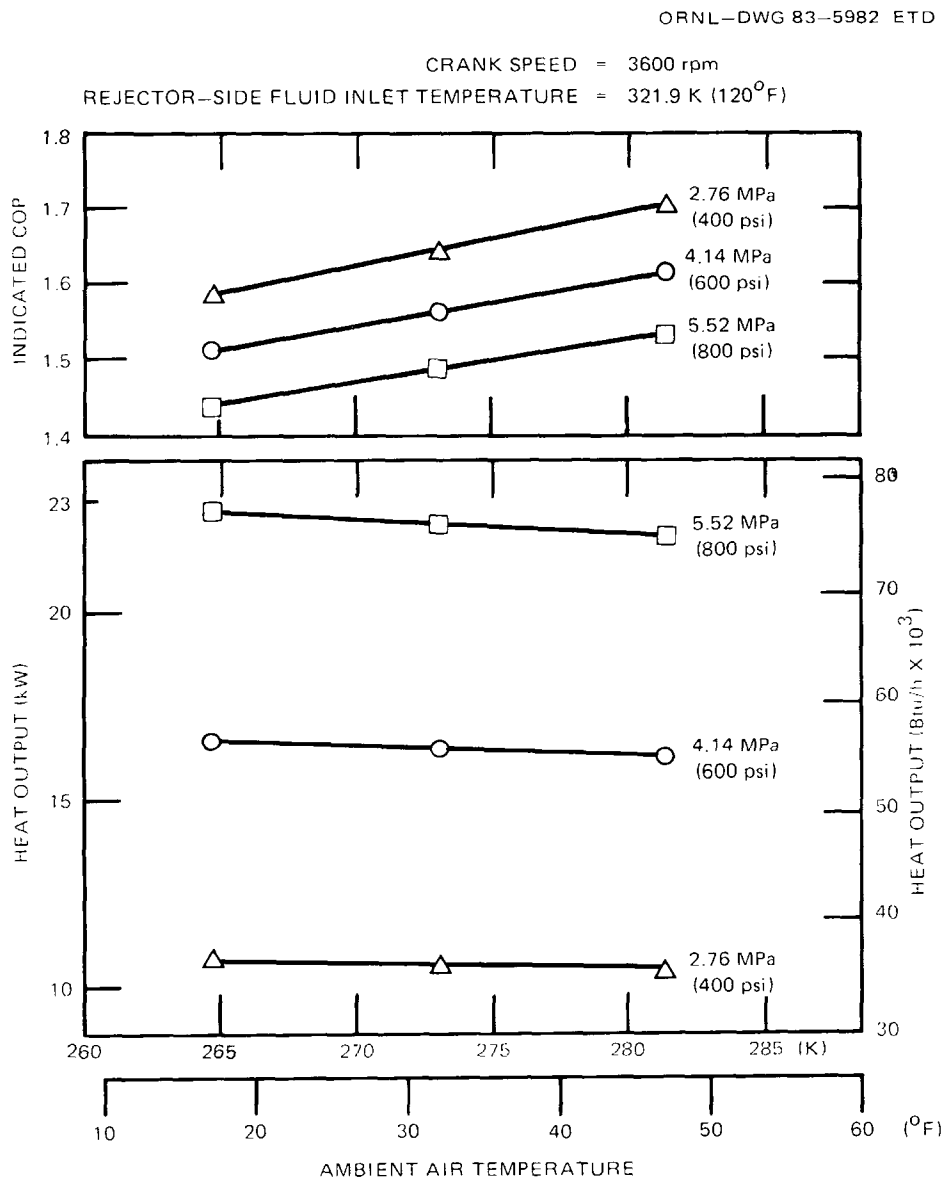

Fig. 13. Performance with modified heat exchangers as function of crank speed and mean compression-space pressure at crank speed of 3600 rpm.

temperature difference was chosen between the ambient air temperature and the heat absorber fluid inlet temperature. It should be noted that higher heat pump performance is achievable by reducing this temperature difference. Figure 20 in Sect. 5.4.6 gives an indication of expected performance levels associated with changes in such temperature difference.

ORNL–DWG 83–5983 ETD

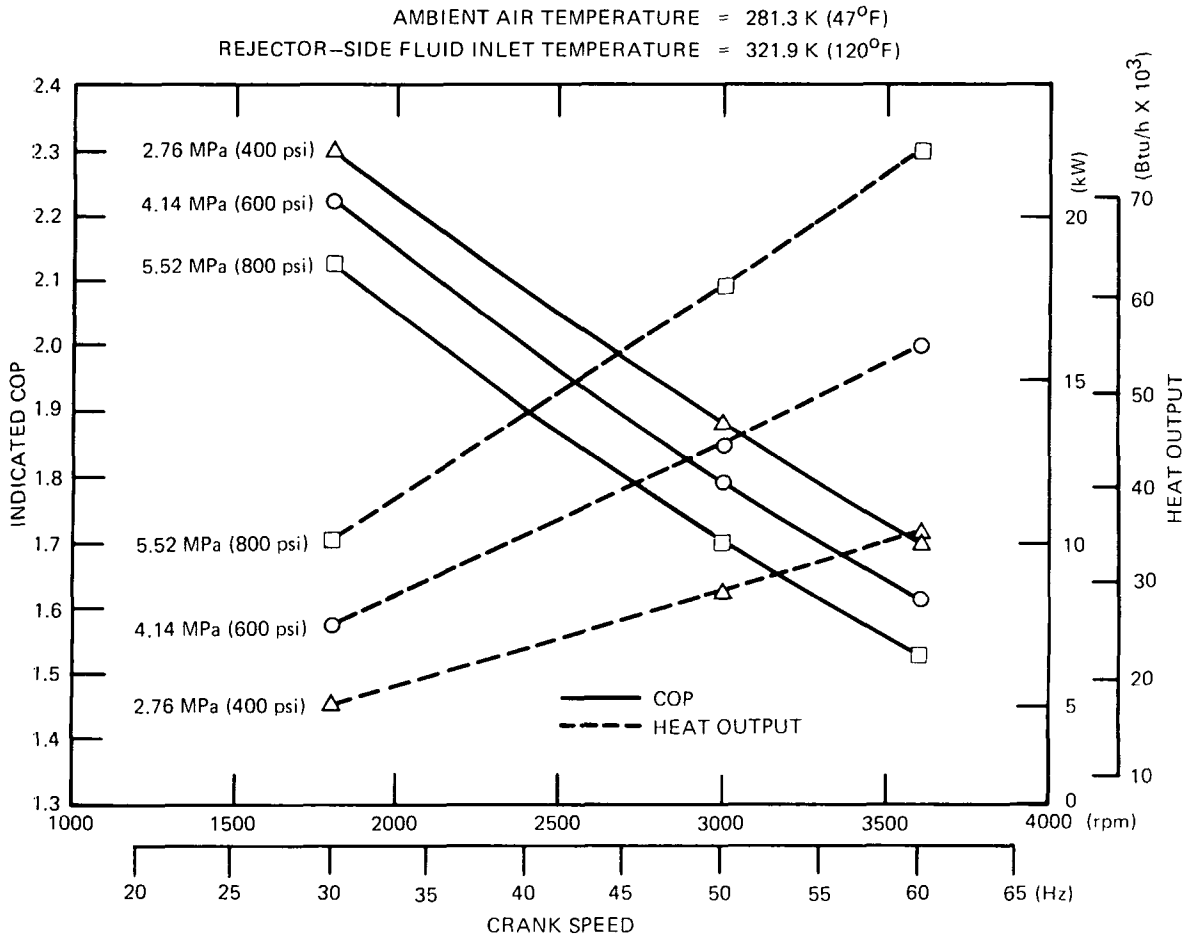

Fig. 14. Performance with modified heat exchangers as function of crank speed and mean compression-space pressure.

Figures 11 through 13 present indicated COP and heat output as a function of ambient air temperature, for a fixed speed and mean compression-space pressure. Figure 14 presents indicated COP and heat output as a function of crank speed for a fixed ambient air temperature and mean compression-space pressure.

5.3.1 Effects of Source (Outdoor Air) Temperature

As illustrated in Figs. 11 through 13, for a constant pressure, COP tended to decrease with decreasing ambient air temperature. However, unlike conventional vapor compression heat pumps, COP for a Stirling-cycle heat pump drops only moderately as ambient air temperature drops. Also,

in contrast to vapor compression systems, the Stirling-cycle heat output remained unsusceptible to changes in ambient air temperature. The low performance sensitivity to outdoor temperature suggests the possible application of Stirling-cycle heat pumps in cold climates.

As shown in Fig. 11, the best range in COP was obtained at a mean compression-space pressure of 2.76 MPa (400 psi) and a crank speed of 1800 rpm. With modified heat exchangers (Base Case III configuration), the COP varied from 2.0 to 2.3 for ambient air temperatures of 264.7 to 281.3 K (17 to 47°F), respectively. A heat output of 5 kW (17,064 Btu/h) remained relatively constant for this range of ambient air temperatures.

5.3.2 Effects of Mean Compression-Space Pressure

Figures 11 through 13 also show the heating COP decrease and heat output increase with increasing pressure levels. As pressure increases for a fixed ambient air temperature, crank speed, and heat rejector-side fluid inlet temperature, the compression-space gas temperature increases while expansion-space gas temperature decreases. Consequently, the COP decreases because of the higher temperature difference between the compression space and expansion space. The increase in heat output with increasing gas pressure is due to the larger mass of working gas in the cycle which must alternately be heated and cooled.

5.3.3 Effects of Crank Speed

Figure 14 shows clearly that heat pump COP decreases and heat output increases as crank speed increases for a fixed ambient air temperature and mean compression-space pressure. At higher speeds, flow losses through the heat exchangers increase. Also, as speed increases, compression-space gas temperature increases while expansion-space gas temperature decreases. As a result of these effects, COP decreases and heat output increases.

5.4 Heat Exchanger Sensitivity Analysis

In this section, simulation results from sensitivity analysis performed on the Stirling-cycle heat pump heat exchangers (excluding the regenerator) are discussed. It is known that by improving heat exchanger

efficiency one can approach isothermal heat transfer. Maintaining the hot (compression) and cold (expansion) spaces of a Stirling-cycle heat pump as nearly isothermal as possible during the heat addition and heat rejection processes yields higher performance. This principle coupled with the idea of converting a GPU-3 heat engine to a heat pump is good reason for investigating the effect of heat exchanger parameters on heat pump performance.

Figures 15 through 20 present the sensitivity of various heat exchanger parameters on Stirling-cycle heat pump performance. These parameters included (1) heat transfer fluid flow passes, (2) heat transfer fluid flow rates, (3) tube number, (4) tube length, (5) heat transfer fluid inlet temperature in the heat rejector, and (6) ambient air to heat absorber-side fluid inlet temperature difference.

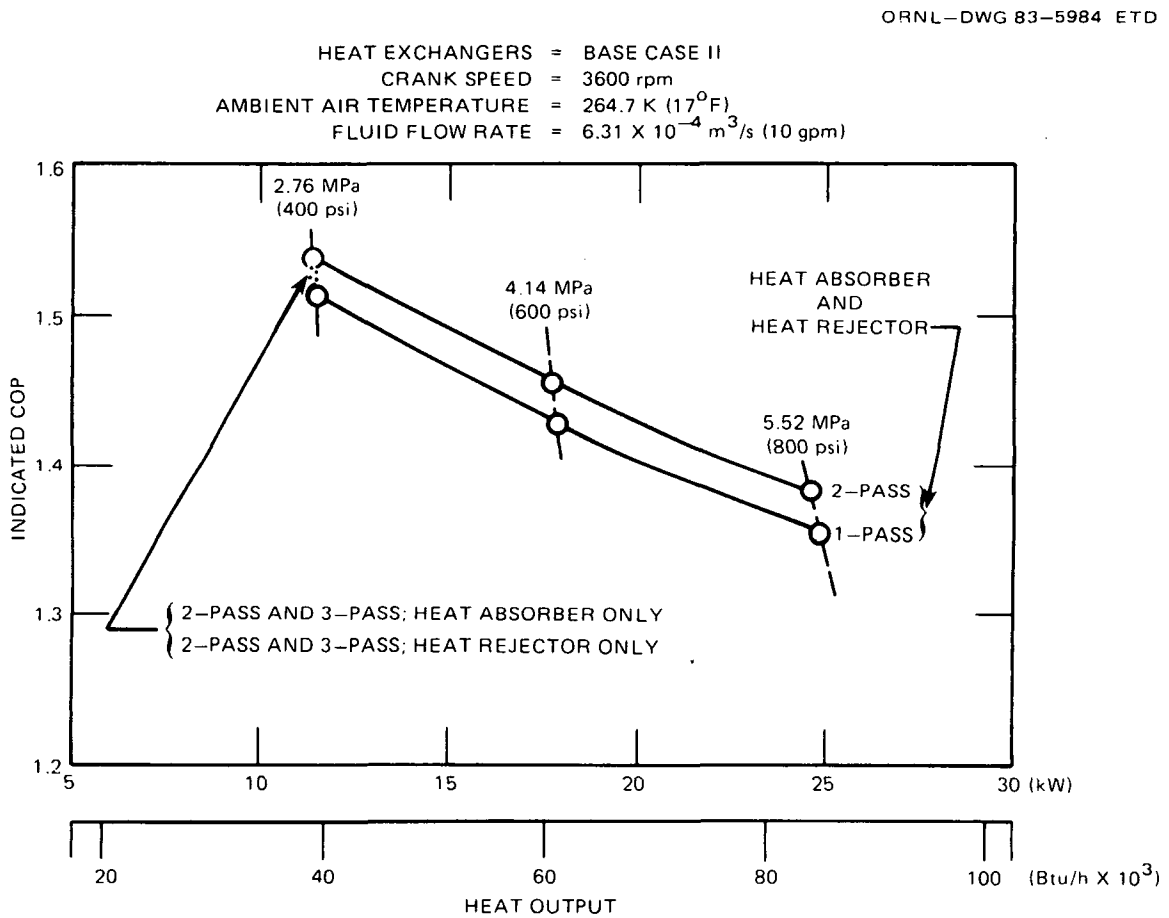

Fig. 15. Sensitivity of heat exchanger shell-side flow passes.

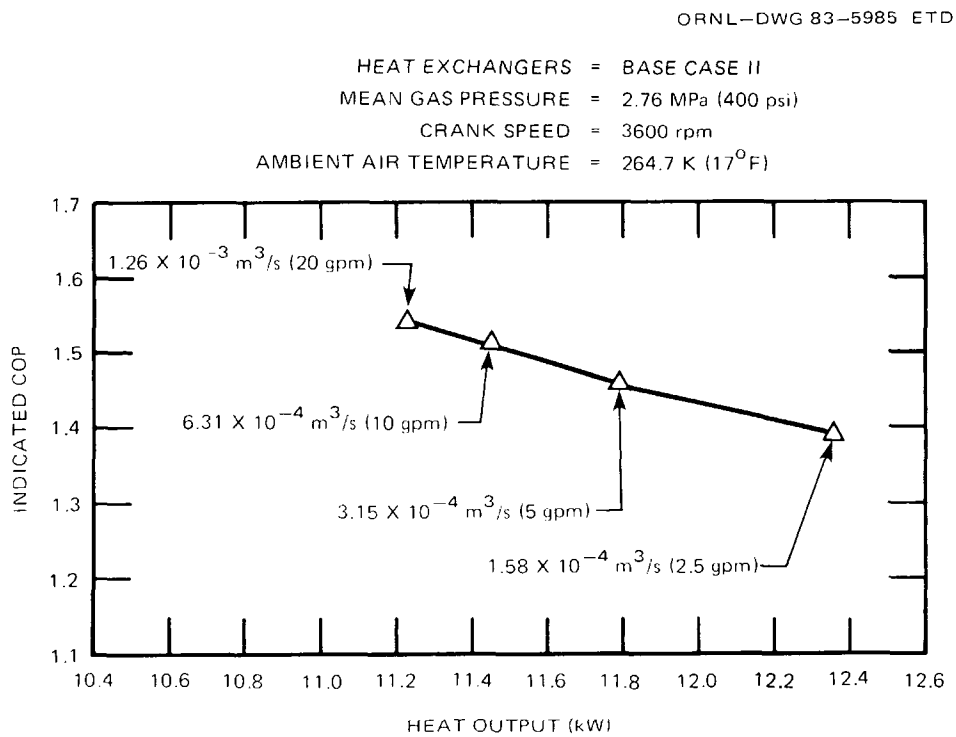

Fig. 16. Sensitivity of heat transfer fluid flow rate.

5.4.1 Effect of Heat Transfer Fluid Flow Passes

Figure 15 illustrates the effect of increasing heat transfer fluid flow passes on the shell-and-tube heat absorber only, the shell-and-tube heat rejector only, and both heat absorber and heat rejector for a given fluid flow rate and inlet temperature. Increasing shell-side flow passes increases heat transfer fluid flow velocities, resulting in higher shell-side heat transfer coefficients. As shown in Fig. 15, doubling the shell-side flow passes on both the heat absorber and heat rejector gave slightly higher performance than individually doubling or tripling the flow passes on both heat exchangers.

Only a 2% increase in COP was achieved at various gas pressure levels using two shell-side flow passes for the heat transfer fluid circulating through the heat absorber and heat rejector. It should be pointed out that increasing shell-side flow passes increases fluid pumping power losses as a result of increasing friction. However, the total pumping loss for both heat exchangers was calculated to be less than 30 W

ORNL–DWG 84–4172 ETD

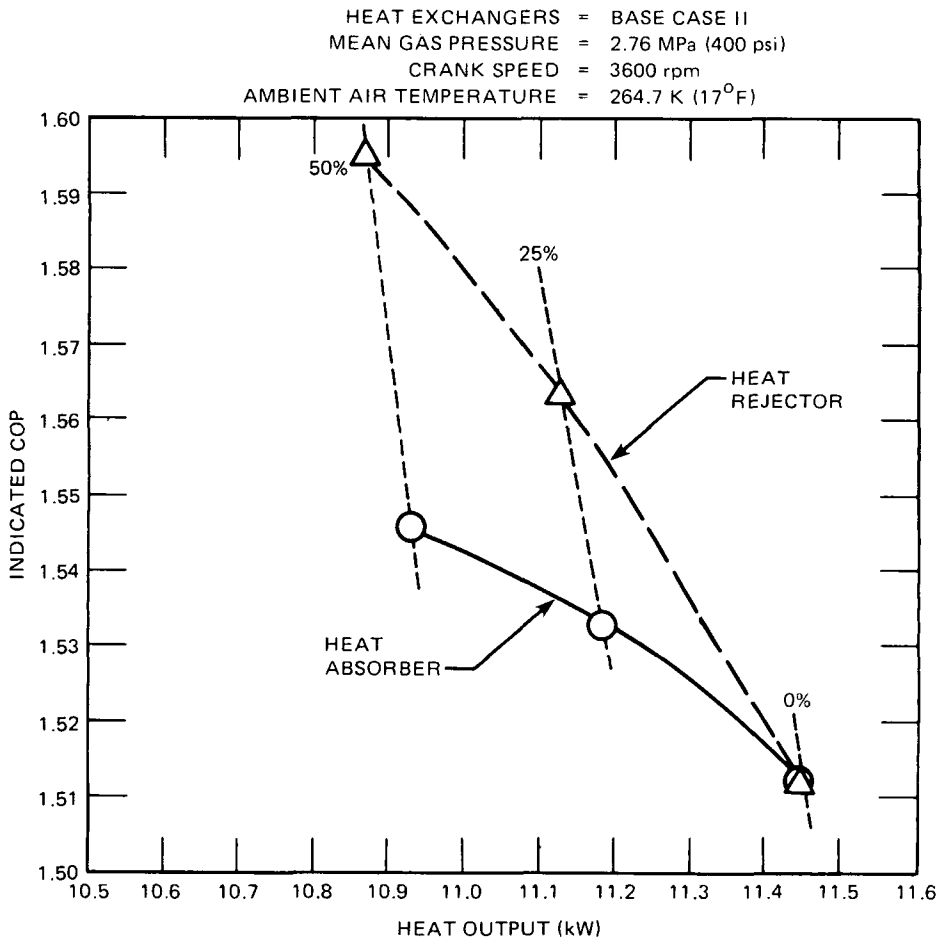

Fig. 17. Sensitivity of heat exchanger tube number increase.

(102.4 Btu/h). It was decided to omit pumping losses from the data shown in Fig. 15, because they appear to be negligible.

Based on the results of Fig. 15, it was decided to modify both heat exchangers to a configuration with two shell-side flow passes (see Table 2 for Base Case III).

5.4.2 Effect of Heat Transfer Fluid Flow Rate

Changes in heating and cooling fluid flow rate were simulated to determine the effect on heat pump performance for a given mean compression-space pressure [2.76 MPa (400 psi)], crank speed (3600 rpm), ambient air

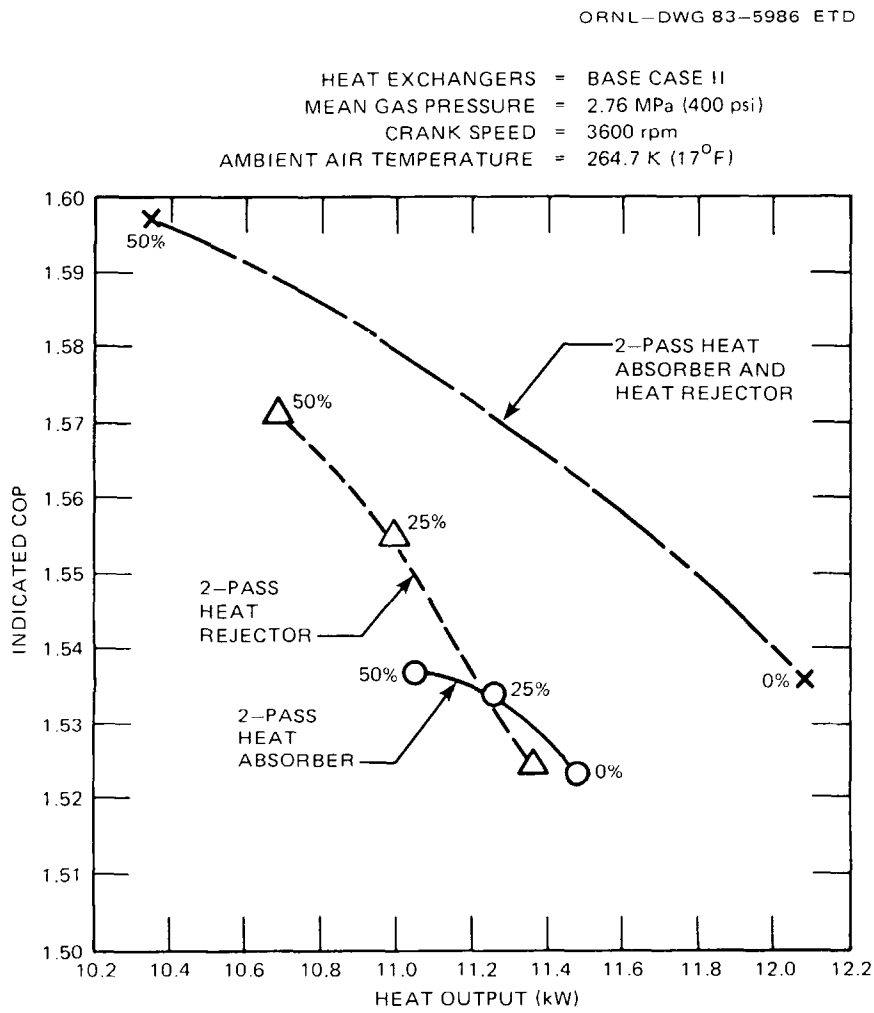

Fig. 18. Sensitivity of heat exchanger tube length increase.

temperature [264.7 K (17°F)], and heat rejection-side fluid inlet temperature [321.9 K (120°F)]. Figure 16 shows indicated COP and heat output as a function of heat transfer fluid flow rate for 1.57×10^{-4}, 3.15×10^{-4}, 6.31×10^{-4}, and 12.62×10^{-4} m^3/s (2.5, 5, 10, and 20 gpm). As flow rate increases, COP and heat output increase. These increases are attributed to higher heat absorber and heat rejector fluid-side heat transfer coefficients due to the higher flow velocities. However, the curve spacing between each flow point shows that as the heat transfer fluid flow rate doubles, the relative gain in performance decreases. This behavior cannot be explained by the effect of pumping power losses because they have been

ORNL–DWG 83–5987 ETD

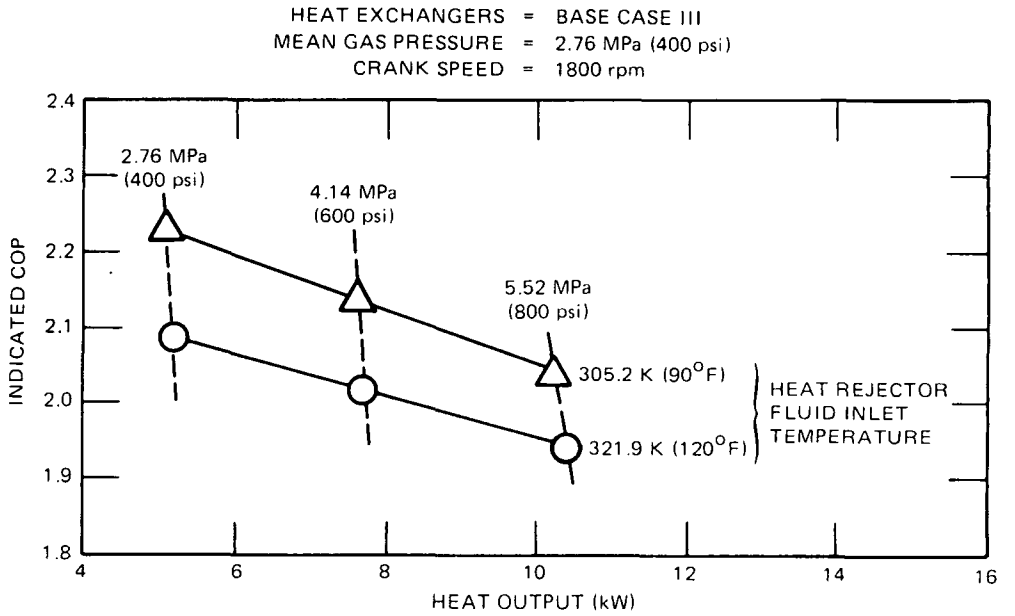

Fig. 19. Sensitivity of changes in heat rejector-side heat transfer fluid inlet temperature.

neglected from the data shown in Fig. 16, but is probably caused by approaching the heat transfer limits of the heat absorber and heat rejector as fluid-side heat transfer coefficients increase with increasing flow rate.

Since the GPU-3 engine was originally designed for a coolant flow rate of $\sim 6.31 \times 10^{-4}$ m^3/s (10 gpm) through the shell-and-tube heat rejector, it was decided to use this value for both heat absorber and heat rejector in the heat pump simulation study.

5.4.3 Effect of Heat Exchanger Tube Number

Figure 17 shows the effect of increasing the number of heat absorber tubes and heat rejector tubes on Stirling-cycle heat pump performance for a given set of operating conditions. For this sensitivity analysis, the Base Case II heat exchangers were modeled. For the heat absorber, the total number of tubes (312) was increased 25% (390) and 50% (468), while the total number of heat rejector tubes remained the same. A similar tube adjustment was made on the heat rejector while keeping the number of heat

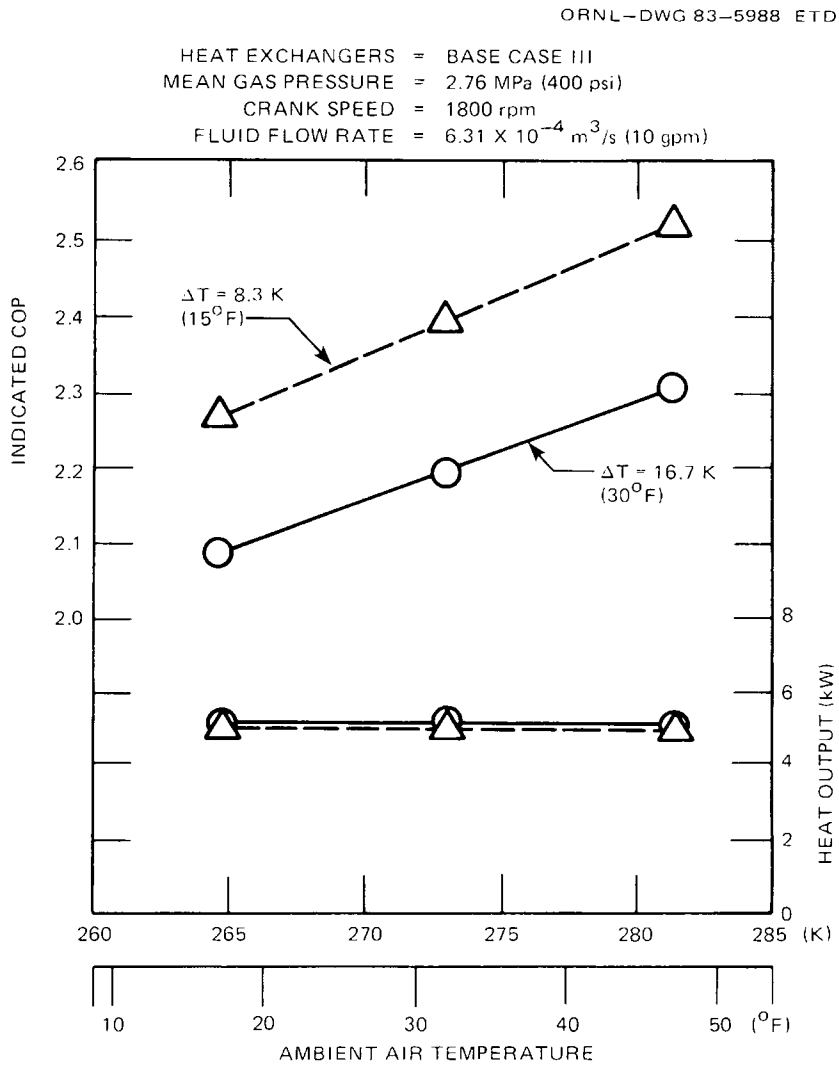

Fig. 20. Sensitivity of ambient air temperature to heat absorber-side heat transfer fluid inlet temperature.

absorber tubes the same. It should be noted that changes in tube number will obviously affect the total surface area, cross-sectional flow area, and volume of a heat exchanger. Therefore, the data shown in Fig. 17 represent the combined effects of these changes. Figure 17 shows that the heat rejector is more sensitive to increases in tube number than is the heat absorber. This is because as a heat pump the heat rejector (originally designed for heat engine applications) must reject a greater amount of heat. As shown in Fig. 17, increasing the number of heat rejector tubes by 50% increases COP by about 5.5% but decreases heat output by a

similar amount (~5.4%). Increasing heat absorber tubes by 50% increases COP by 2.2% but decreases heat output by 4.8%.

5.4.4 Effect of Heat Exchanger Tube Length

Figure 18 shows the effect of an increase in tube length on the heat absorber, heat rejector, and both the heat absorber and heat rejector. An arrangement with two shell-side flow passes for the heat transfer fluid was used for the particular heat exchanger under investigation. If only heat absorber tube length was to be increased, then only the heat absorber portion of the heat exchangers utilized two shell-side flow passes. As shown in Fig. 18, tube length was increased up to 50% for each case, which meant that both heat transfer surface area and volume were increased by 50%.

The highest increase in COP (~4%) was computed when both heat absorber and heat rejector tube lengths were increased 50%. However, the heat output decreased by about 10% for this case. Increasing only the heat absorber tube length did not provide significant improvement in COP. This finding is similar to that reported for the heater in the previous section when the tube number was increased 50%. It appears that the shell-and-tube heat absorber is adequately sized for the Stirling-cycle heat pump.

For the heat rejector, increasing tube length by 50% gave an increase in COP of 3.1% and a decrease in heat output of 6.3%. A comparison of Figs. 17 and 18 shows that a slightly higher COP can be achieved by increasing the tube number in the heat rejector rather than tube length. However, increasing the number of tubes in the heat rejector introduces the complexity of redesigning the heat rejector—regenerator—heat absorber cartridges (Figs. 3 through 5) along with the cylinder head because the diameters of these components will undoubtedly change. Of course, added complexity also results in increased costs, a factor which cannot be ignored.

In order to keep the Stirling-cycle heat pump design relatively simple, it was decided to improve the performance by increasing the length of heat rejector tubes by 50%. This change led to our Base Case III configuration.

5.4.5 Effect of Heat Rejector-Side Heat Transfer Fluid Inlet Temperature

The effect of heat transfer fluid inlet temperature flowing through the heat rejector on Stirling-cycle heat pump performance is shown in Fig. 19. This parameter may be viewed as the inlet temperature of a delivery fluid used for space heating and/or process water heating. In Fig. 19, indicated COP and heat output are shown for various mean compression-space pressure levels.

Computer runs were made at fluid inlet temperatures of 305.2 and 321.9 K (90 and 120°F) for a fixed crank speed (1800 rpm), ambient outdoor air temperature [264.7 K (17°F)], and heating and cooling flow rates of 6.31×10^{-4} m^3/s (10 gpm). The Base Case III heat exchanger configuration was used in this analysis, based on the favorable findings reported in previous sections.

As expected, the results indicate an increase in COP as heat rejector-side fluid inlet temperature is lowered. This is so because as fluid temperature decreases the gas temperature flowing through the heat rejector decreases. Since the heat absorber operating conditions have not changed, the Stirling-cycle heat pump is able to operate with less power at a lower temperature difference between the heat rejector and heat absorber portions; therefore, COP increases. As shown in Fig. 19, lowering the fluid inlet temperature by 16.7 K (30°F) increases COP from 5 to 7% as gas pressure decreases. The heat output appears to decrease very slightly, for the same pressure.

5.4.6 Effect of Temperature Difference Between Outdoor Air and Absorber-Side Heat Transfer Fluid Inlet Temperature

Most simulation results presented in earlier sections were obtained by choosing a very conservative temperature difference between (1) the ambient outdoor air temperature and heat absorber-side heat transfer fluid inlet temperature and (2) the heat rejector-side heat transfer fluid inlet temperature and indoor air exit temperature. Consequently, the Stirling-cycle heat pump operated at a higher temperature difference between the heat rejector and heat absorber portions, resulting in lower COP.

Figure 20 illustrates the effect of decreasing ambient air (source) temperature to heat absorber fluid inlet temperature on Stirling-cycle heat pump performance for fixed gas pressure, crank speed, and fluid flow rates. By decreasing this temperature difference by half [ΔT = 8.3 K (15°F)] the COP increases up to 9.7%, yet the heat output remains practically unchanged at about 5 kW (17,064 Btu/h).

REFERENCES

1. G. Walker, *Stirling-Cycle Machines*, Clarendon Press, Oxford, 1973.

2. A. A. Domingorena, *Performance Evaluation of a Low-First-Cost, 3-Ton, Air-to-Air Heat Pump in the Heating Mode*, ORNL/CON-18, Union Carbide Corp., Nuclear Div., Oak Ridge Natl. Lab., 1978.

3. F. A. Creswick, "Alternative Heat Pump Cycle Studies," *Proceedings of the DOE Heat Pump Contractors' Program Integrating Meeting, June 2—4, 1981.*

4. *A Collection of Stirling Engine Reports from General Motors Research, 1958—1970*, Research Publication GMR-2690 (Publication arranged by NASA Lewis Research Center with permission from General Motors Research Labs; available from NTIS), 1978.

5. L. G. Thieme, *Low-Power Baseline Test Results for the GPU-3 Stirling Engine*, DOE/NASA/1040-79/6, NASA TM-79103, U.S. DOE, April 1979.

6. L. G. Thieme, *High-Power Baseline and Motoring Test Results for the GPU-3 Stirling Engine*, DOE/NASA/51040-31, NASA TM-82646, U.S. DOE, June 1981.

7. W. R. Martini, *Stirling Engine Design Manual*, NASA CR-135382, April 1978.

8. C. D. West, *The Stirling Engine with One Adiabatic Cylinder*, ORNL/TM-8022, Union Carbide Corp., Nuclear Div., Oak Ridge Natl. Lab., March 1982.

9. W. R. Martini, *Design Study of Isothermalized Stirling Engines*, Final Report: ANL Contract 31-109-38-5304, September 1980.

10. G. M. Benson, "Thermal Oscillators," 1977 IECEC Record, Paper 779247, pp. 1478—87.

11. R. Tew, K. Jefferies, and D. Miao, *A Stirling Engine Computer Model for Performance Calculations*, DOE/NASA/1011-78/24, NASA TM-78884, U.S. DOE, July 1978.

12. R. C. Tew, L. G. Thieme, and D. Miao, *Initial Comparison of Single Cylinder Stirling Engine Computer Model Predictions with Test Results*, DOE/NASA/1040-78/30, NASA TM-79044, U.S. DOE, July 1979.

Appendix A

INTRODUCTION TO STIRLING-CYCLE HEAT PUMPS

The Stirling-cycle heat pump analyzed in this study can be described as a closed-cycle piston heat pump with cyclic recirculation of the working fluid. Heat is absorbed by the working gas at some temperature lower than the ambient, and shaft work is added. The absorbed heat and the shaft work are converted into the internal energy of the working gas, which is rejected to the surroundings at a temperature above the ambient.

During heat pump operation, a power piston compresses the working gas at a high temperature. The gas is then cooled, expanded at a low temperature, and heated again. In the Stirling-cycle heat pump, the required heat is applied to the working gas from the outside through a wall. Because of the high heat capacity of the wall, the gas cannot be heated and cooled simply by rapid heating and cooling of the wall. Therefore, a second piston, called the displacer, is added to the machine to move the gas between two stationary chamber volumes called the hot space and the cold space. To avoid unnecessary waste of heat during the alternating heating and cooling processes, a regenerator is placed between the hot (heat rejector) and cold (heat absorber) heat exchangers. This regenerator is a space filled with a porous material that cools the gas before it moves toward the cold space (expansion space). On its return, the stream of gas reabsorbs the stored heat before reentering the hot space (compression space). A Stirling-cycle heat pump machine in its simplest form is shown in Fig. A.1.

A.1 Ideal Stirling-Cycle Heat Pump

The ideal Stirling-cycle heat pump cycle is shown in the pressure-volume (P-V) and temperature-entropy (T-S) diagrams of Fig. A.2(*a*).

1. Process 1 → 2 is an isothermal compression in which heat is transferred from the working fluid at the maximum cycle temperature to the external sink (heat rejected from the Stirling-cycle heat pump).

ORNL–DWG 83–5989 ETD

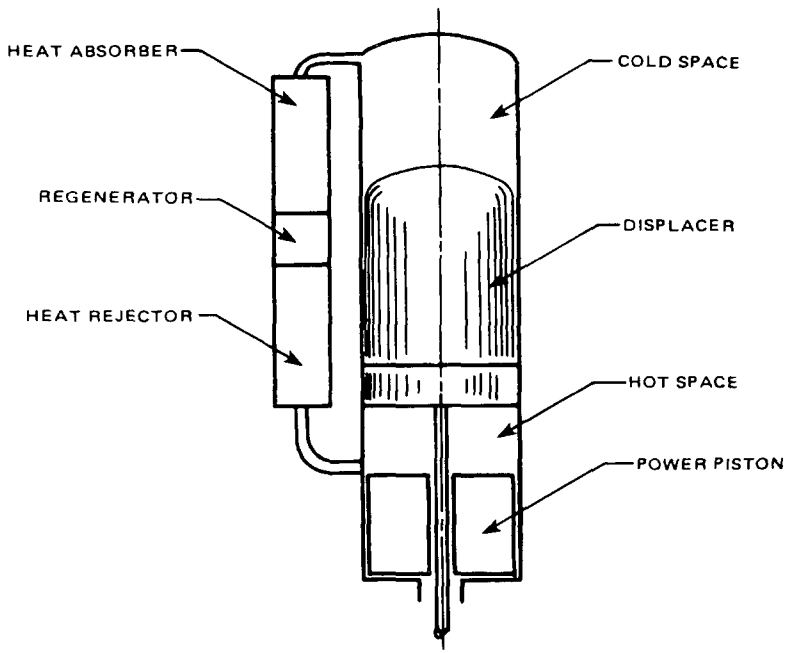

Fig. A.1. Typical Stirling-cycle heat pump.

ORNL–DWG 83–4639R ETD

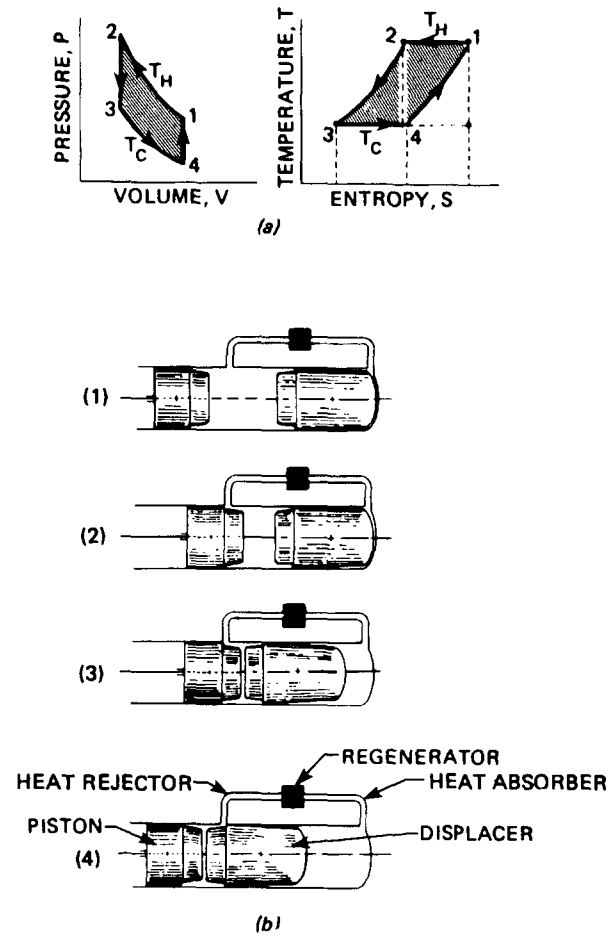

Fig. A.2. Stirling-cycle heat pump: (*a*) P–V and T–S diagrams and (*b*) piston positions at state points of the cycle.

2. Process 2 → 3 is a constant-volume regenerative process in which heat is transferred to the regenerator matrix from the working fluid (heat absorbed).
3. Process 3 → 4 is an isothermal expansion in which heat is transferred to the working fluid at the minimum cycle temperature from the external source (heat added to the Stirling-cycle heat pump).
4. Process 4 → 1 is a constant-volume regenerative process in which heat is transferred to the working fluid from the regenerator matrix (heat released).

Figure A.2(*b*) shows the operation of a Stirling-cycle heat pump. At the beginning of the cycle, the power piston is at its bottom dead center point, and the displacer piston is at its top dead center point. All of the working fluid is in the compression (hot) space. This starting point corresponds to point 1 in the P-V and T-S diagrams of Fig. A.2 where the volume and fluid temperature are at their maximum levels.

With the displacer piston stationary, the power piston moves toward the top dead center point (process 1 → 2), compressing the working fluid isothermally. Since heat is being rejected from the compression space to the surroundings, the temperature remains constant. Because the working fluid is compressed, the pressure increases.

With the power piston remaining stationary in its top dead center position, the displacer piston advances toward the power piston, moving the working fluid at constant volume from the hot compression space through the porous regenerator matrix to the cold expansion space (process 2 → 3). Heat is transferred to the regenerator matrix from the fluid, thereby decreasing the fluid temperature. The decrease in fluid temperature causes a decrease in pressure.

The displacer piston continues to move away from its top dead center point as the isothermal expansion process (process 3 → 4) progresses. Pressure decreases as volume increases, but the fluid temperature is kept constant since heat from an external source is being added to the expansion space.

The final process in the cycle is completed as the displacer piston transfers the working fluid at constant volume from the cold expansion

space through the regenerator matrix to the hot compression space, while the power piston remains stationary (process 4 → 1). Heat is transferred from the regenerator matrix to the working fluid, thus increasing the fluid temperature and pressure. The heat depleted from the regenerator matrix is the heat stored there during process 2 → 3 of the cycle.

If the heat that is transferred to the working fluid from the regenerator matrix is the same as that transferred from the fluid to the matrix, then only the external heat transfer processes remain, and the performance is the same as the Carnot cycle. Theoretically, Stirling-cycle machines offer the best possible means to utilize thermal resources. However, the actual performance of a Stirling-cycle machine, affected by irreversibilities in heat transfer and mechanical friction losses, may attain only a fraction of the ideal value.

A.2 Departures from the Ideal Cycle

The ideal cycle described assumes that the processes are thermodynamically reversible; in other words, the expansion and compression processes are isothermal, and infinite heat rates exist in addition to infinite heat capacities. In the ideal analysis, the effects of regenerator matrix voids, clearance spaces, and cylinder pockets were neglected. In addition, the pistons were assumed to move in a discontinuous manner, whereas in reality the motion is a smooth, continuous path. Therefore, in reality, the theoretical P-V and T-S diagrams are rounded off. Aerodynamic and mechanical losses were also neglected. Inclusion of these losses, of course, results in a higher net cycle input power and lower efficiency.

The addition of the heat exchanger components changes the real heat transfer to a more adiabatic process rather than the assumed isothermal processes. Penalties in additional aerodynamic flow losses and increased dead volume result.

Appendix B

SI CONVERSION FACTORS

An attempt has been made to present all key tables and figures in dual units (ACU and SI). The following conversion factors may be used to convert from ACU to SI units:

To convert from	To	Multiply by
Btu/h	W	0.2929
Btu/h•ft^2	W/m^2	3.152
Btu/h•ft•°F	W/m•K	1.730
Btu/h•ft^2•°F	W/m^2•K	5.675
Btu/lb$_m$	J/kg	2.234×10^3
Btu/lb$_m$•°F	J/kg•K	4.184×10^3
ft	m	0.3048
ft^2	m^2	0.0929
ft/h^2	m/s^2	2.35×10^{-8}
ft/s	m/s	0.3048
gpm	m^3/s	6.309×10^{-5}
in.	cm	2.54
lb$_f$/ft	N/m	14.59
lb$_m$/ft^3	kg/m^3	16.02
lb$_m$/h•ft	Pa•s	4.134×10^{-4}
lb$_m$/h•ft^2	Pa•s/m	1.356×10^{-3}
psi	Pa	6.895×10^3
Δ(°F)	Δ(K) or Δ(°C)	0.5556
Temperature conversion	T(K) = 5/9 x [T(°F) — 32] + 273 T(°C) = 5/9 x [T(°F) — 32]	

ORNL/CON-149
Dist. Category UC-95d

Internal Distribution

1. V. D. Baxter
2-6. F. C. Chen
7. N. C. J. Chen
8. G. E. Courville
9. F. A. Creswick
10. J. L. Crowley
11. R. C. DeVault
12-16. N. Domingo
17. R. D. Ellison
18. P. D. Fairchild
19. S. K. Fisher
20. W. Fulkerson
21. F. P. Griffin
22. D. S. Griffith
23. V. O. Haynes
24. K. E. Heidenreich
25. H. W. Hoffman
26-30. W. L. Jackson
31. S. I. Kaplan
32. S. V. Kaye (Consultant)
33. T. R. La Porte (Consultant)
34. W. P. Levins
35. V. C. Mei
36. J. W. Michel
37. W. A. Miller
38. R. E. Minturn
39. L. I. Moss (Consultant)
40. R. W. Murphy
41. E. A. Nephew
42. H. Perez-Blanco
43. G. T. Privon
44. C. K. Rice
45. M. Russell (Consultant)
46. H. E. Trammell
47. E. A. Vineyard
48. C. D. West
49. W. H. Williams (Consultant)
50. ORNL Patent Office
51. Central Research Library
52. Document Reference Section
53-54. Laboratory Records Department
55. Laboratory Records (RC)

External Distribution

56. W. T. Beale, Sunpower, Inc., 6 Byard St., Athens, OH 45701
57. G. M. Benson, Energy Research and Generation, Inc., Lowell and 57th Street, Oakland, CA 94608
58. Donald G. Beremand, Stirling Engine Project Office, National Aeronautics and Space Administration, Lewis Research Center, Cleveland, OH 44135
59. James E. Calm, Project Manager, Heat Pump Development, Electric Power Research Institute, 3412 Hillview Avenue, P.O. Box 10412, Palo Alto, CA 94303
60. Stig G. Carlqvist, Societe ECA, 17, avenue du Chateau, 92190 Meudon-Bellevue, France
61. W. S. Chiu, Systems Engineering, General Electric Company, P.O. Box 527, King of Prussia, PA 19406
62. J. G. Daley, Argonne National Laboratory, 9700 South Cass Avenue, Argonne, IL 60439
63. G. Dochat, Mechanical Technology, Inc., 968 Albany-Shaker Rd., Latham, NY 12110
64. T. Finkelstein, TCA, P.O. Box 643, Beverly Hills, CA 90213

65. R. J. Fiskum, Program Manager, Energy Conversion Equipment Branch, CE113.2, Rm. GH068, Department of Energy, 1000 Independence Ave. S.W., Washington, DC 20585
66. D. R. Gedeon, Sunpower, Inc., 6 Byard St., Athens, OH 45701
67. L. Goldberg, University of Minnesota, The Underground Space Center, 11 Mines and Metallurgy, 221 Church Street, SE, Minneapolis, MN 55455
68. T. J. Heames, Argonne National Laboratory, 9700 South Cass Avenue, Argonne, IL 60439
69. F. W. Hoehn, Rockwell International Corp., 6633 Canoga Avenue, Canoga Park, CA 91304
70. J. Hogan, General Electric Co., P.O. Box 8666, Philadelphia, PA 19101
71. R. E. Holtz, Components Technology Division, Bldg. 330, Argonne National Laboratory, 9700 South Cass Ave., Argonne, IL 00439
72. Y. Ishizaki, Cryogenic Systems, 253-5 Yamanouchi, Kamakura 247, Japan
73. Naotsugu Isshiki, 2-29-6 Kyodo Setagayaku, Tokyo 156, Japan
74. T. Kapus, Energy Conversion Equipment Branch, CE 113.2, Department of Energy, 1000 Independence Ave. S.W., Washington, DC 20585
75. Prof. Nobuhide Kasagi, University of Tokyo, Dept. of Mechanical Engineering, Bunkyo-Ku, Tokyo 113, Japan
76. V. H. Larson, Cleveland State University, 1983 East 24th St., Cleveland, OH 44115
77. K. P. Lee, Manager, Facility and Manufacturing Automation, P.O. Box 809, Sudbery, MA 01776
78. W. Martini, Martini Engineering, 2303 Harris, Richland, WA 99352
79. R. C. Meijer, Advanced Energy Programs Dept., General Electric Company, P.O. Box 527, King of Prussia, PA 19406
80. G. McLennan, Argonne National Laboratory, 9700 South Cass Avenue, Argonne, IL 60439
81. N. P. Nightingale, Stirling Engine Systems Division, Mechanical Technology, Inc., 968 Albany-Shaker Rd., Latham, NY 12110
82. Herbert Nilsson, United Stirling AB, Box 856, S-201 80 Malmo, Sweden
83. W. Perceval, United Stirling, Inc., 211 Strand, Alexandria, VA 22314
84. C. J. Rallis, University of Witwatersrand, School of Mechanical Engineering, 1 Jan Smuts Avenue, Johannesburg 2001, South Africa
85. G. Rice, Department of Engineering, The University of Reading, Reading, Berkshire, England
86. W. D. Rifkin, Energy Research and Generation, Inc., Lowell and 57th Street, Oakland, CA 94608
87. A Ross, Ross Enterprises, 37 West Broad Street, Suite 360, Columbus, OH 43215
88. J. D. Ryan, Acting Chief, Energy Conversion Equipment Branch, CE113.2, Rm. GH068, Department of Energy, 1000 Independence Ave. S.W., Washington, DC 20585
89. A. Schock, Fairchild Industries, Germantown, MD 20874
90. J. Schuster, Gas Research Institute, 8600 W. Bryan Mawr Ave., Chicago, IL 60631

91. R. Shoureshi, Department of Mechanical Engineering, College of Engineering, Wayne State University, Detroit, MI 48202
92. D. J. R. Senft, Department of Mathematics/Computer Science, University of Wisconsin, River Falls, WI 54022
93. J. L. Smith, Jr., Mechanical Engineering Department, Massachusetts Institute of Technology, Cambridge, MA 02139
94. J. G. Slaby, National Aeronautics and Space Administration, Lewis Research Center, Cleveland, OH 44135
95. D. R. Taylor, Royal Naval Engineering College, Manadon Plymouth, Devon PL5 3AQ, England
96. W. P. Teagan, Arthur D. Little, Inc., Acorn Park, Cambridge, MA 02140
97. R. C. Tew, NASA-Lewis Research Center, 21000 Brookpark Rd., Cleveland, OH 44135
98. L. G. Thieme, NASA-Lewis Research Center, 21000 Brookpark Rd., Cleveland, OH 44135
99. I. Urieli, Sunpower, Inc., 6 Byard St., Athens, OH 45701
100. Valerie J. Van Griethuysen, Energy Conversion Branch, Aerospace Power Division — Aero Propulsion Laboratory, Dept. of the Air Force, Wright-Patterson AFB, OH 45433
101. G. Walker, University of Calgary, Dept. of Mechanical Engineering, 2920 24th Ave., NW, Calgary, Canada T2N1N4
102. B. P. Wang, Mechanical Engineering Department, University of Texas at Arlington, P.O. Box 19023, Arlington, TX 76019
103. M. A. White, University of Washington, Joint Center for Graduate Study, 100 Sprout Road, Richland, WA 99352
104. L. Williams, Logan Lewis Library, Research Division, Carrier Corporation, Carrier Parkway, Syracuse, NY 13221
105. Office of Assistant Manager for Energy Research and Development, Department of Energy, ORO, Oak Ridge, TN 37830

106-363. Given distribution as shown in DOE/TIC-4500 under category UC-95d (Energy Conservation — Buildings and Community Systems)

☆U.S. GOVERNMENT PRINTING OFFICE: 1983-646-055/288